

Towards Unified AI Models for MU-MIMO Communications: A Tensor Equivariance Framework

Yafei Wang, *Graduate Student Member, IEEE*, Hongwei Hou, *Graduate Student Member*,
Xinping Yi, *Member, IEEE*, Wenjin Wang, *Member, IEEE*, Shi Jin, *Fellow, IEEE*

Abstract—In this paper, we propose a unified framework based on equivariance for the design of artificial intelligence (AI)-assisted technologies in multi-user multiple-input-multiple-output (MU-MIMO) systems. We first provide definitions of multidimensional equivariance, high-order equivariance, and multidimensional invariance (referred to collectively as tensor equivariance). On this basis, by investigating the design of precoding and user scheduling, which are key techniques in MU-MIMO systems, we delve deeper into revealing tensor equivariance of the mappings from channel information to optimal precoding tensors, precoding auxiliary tensors, and scheduling indicators, respectively. To model mappings with tensor equivariance, we propose a series of plug-and-play tensor equivariant neural network (TENN) modules, where the computation involving intricate parameter sharing patterns is transformed into concise tensor operations. Building upon TENN modules, we propose the unified tensor equivariance framework that can be applicable to various communication tasks, based on which we easily accomplish the design of corresponding AI-assisted precoding and user scheduling schemes. Simulation results demonstrate that the constructed precoding and user scheduling methods achieve near-optimal performance while exhibiting significantly lower computational complexity and generalization to inputs with varying sizes across multiple dimensions. This validates the superiority of TENN modules and the unified framework.

Index Terms—Artificial intelligence, tensor equivariance, unified framework, MU-MIMO transmission.

I. INTRODUCTION

THE multiple-input-multiple-output (MIMO) technology [1], which serves users using multiple antennas, has become a key technology in wireless communication systems due to its enormous potential for increasing system capacity [2]. Leveraging MIMO technology, the base stations (BSs) in multi-user MIMO (MU-MIMO) systems possess enhanced transmission performance to simultaneously serve multiple users. In such systems, resource allocation schemes such as user scheduling and precoding techniques play a important role in improving throughput. On the one hand, user scheduling aims to select users from the pool of all users for simultaneous

transmission in certain resource elements, with the goal of improving transmission quality. On the other hand, precoding further enhances the potential capacity gains by suppressing user interference. Since the evolution of MU-MIMO technology, numerous excellent scheduling and precoding algorithms have been proposed, such as greedy-based scheduling schemes [3] and weighted minimum mean square error (WMMSE) precoding [4]–[6].

While conventional transmission schemes in MU-MIMO systems can achieve outstanding performance [3], [4], even approaching the performance limits [7], [8], they usually require iterative computations and high computational complexity. Such issues become increasingly severe in the face of the growing scale of wireless communication systems [9], posing obstacles to their application in practical systems. In contrast, artificial intelligence (AI) models possess the potential to accelerate iterative convergence and approximate high-dimensional mappings with lower computational complexity [10], [11], leading to extensive research into AI-assisted transmission schemes [12].

Most AI-assisted transmission schemes treat inputs as structured data, such as image data or vector data, and process them using corresponding neural networks (NNs) [13]–[18]. Specifically, building on the optimal closed-form solution derived from WMMSE precoding [4], [19], the authors in [13] utilize fully connected (FC) layers to directly compute key features in optimal solution forms, while similar schemes are proposed with convolutional NN (CNN) in [14] and [15], as channel information can be regarded as image data. Based on CNN, AI-assisted schemes utilizing optimal solution structures have been extended to multiple precoding optimization criteria [16]. With the imperfect channel state information (CSI), [17] and [18] investigated the robust WMMSE precoding algorithms with CNNs. Unlike FC and CNN networks, deep unfolding networks integrate learnable parameters into iterative algorithms to expedite algorithmic convergence [20]–[22]. For instance, [20] introduced a matrix-inverse-free deep unfolding network for WMMSE precoding. A similar approach is explored in [21], demonstrating better performance compared to CNNs. Such approach is further extended to WMMSE precoding design under imperfect CSI conditions [22]. Apart from precoding, there are also some AI-assisted methods for other resource allocation schemes [23]–[25]. In [23], FC networks are utilized to extract optimal power allocation schemes from CSI for maximizing sum-rate. Besides, a user

Manuscript received xxx.

Yafei Wang, Hongwei Hou, and Wenjin Wang are with the National Mobile Communications Research Laboratory, Southeast University, Nanjing 210096, China, and also with Purple Mountain Laboratories, Nanjing 211100, China (e-mail: wangyf@seu.edu.cn; hongweihou@seu.edu.cn; wangwj@seu.edu.cn).

Xinping Yi and Shi Jin are with the National Mobile Communications Research Laboratory, Southeast University, Nanjing 210096, China (e-mail: xiyi@seu.edu.cn; jinshi@seu.edu.cn).

scheduling strategy aided by FC networks is proposed in [24], which assigns the most suitable single user for each resource block. Based on edge cloud computing and deep reinforcement learning, the user scheduling strategy in [25] are developed for millimeter-wave vehicular networks. Additionally, there are studies providing novel ideas to understand and assist in the design of AI-assisted methods in wireless communications [26], [27]. The work in [26] elucidates the shortcomings of AI in solving non-convex problems and presents a framework to address this issue. The authors of [27] investigated the asymptotic spectral representation of linear convolutional layers, offering guidance on the excellent performance of CNNs.

The aforementioned studies typically do not focus on permutation equivariance (abbreviated as equivariance) [28], which entails that permutation of input elements in a model also results in the corresponding permutation of output elements. Such property is inherent to MU-MIMO systems and endows AI-assisted transmission technologies with the potential advantages like parameter sharing [29]. Benefiting from its modeling of graph topology, graph NN (GNN) possess the capability to exploit this property, thus being employed in the design of transmission schemes and demonstrating outstanding performance [30]. In [31], the significance of topological information for transmission within an interference management framework is investigated. The GNNs used for wireless resource management is proposed in [32], which develops equivariance and thereby achieves generalization across varying numbers of users. In addition, the authors in [33] model the link network between BS antennas and terminals as a bipartite graph, thereby achieving generalization across varying numbers of users and BS antennas. Similarly, GNNs with different iteration mechanisms are proposed for precoding design in [34] and [35]. By crafting refined strategies for updating node features, a GNN satisfying equivariance across multiple node types is devised for hybrid precoding in [36]. This work also reveals various potential scenarios and tasks for the proposed GNN method. The proposed methodology demonstrates exceptional performance and scalability, paving the way for GNN-assisted transmission design. Furthermore, aiming to maximize the number of served users, a GNN-based joint user scheduling and precoding method is investigated in [37].

Existing efforts in developing inherent properties in wireless communication systems are limited to GNN, requiring intricate node modeling and the construction of node update strategy during the design process. Therefore, with the increasing trend of incorporating multiple device types in communication systems [38], the design of schemes based on this approach may become increasingly complicated. Furthermore, although existing work has made contributions in developing equivariance in communication systems [36], [39], [40], there is little effort on investigating concise and unified frameworks to develop diverse equivariances such as multidimensional equivariance [41], higher-order equivariance [42], and invariance [43] in such systems.

In this paper, we focus on the development of these properties and proposed a unified framework for exploiting them in MU-MIMO systems. The major contributions of our work

are summarized as follows:

- **Framework:** We propose the tensor equivariance (TE) framework for MU-MIMO transmission, which consists of four key components: *mathematical foundation, module design, case study, and experimental validation*. This framework facilitates the development of TE in AI-assisted MU-MIMO transmission schemes.
- **Mathematical Foundation:** We explore the most valuable permutation equivariance/invariance properties and their variations (collectively referred to as TE) in MU-MIMO transmission through rigorous and concise mathematical definitions, thereby treating most past works as special cases of our approach. On the basis, we transform the research paradigm from topological modeling based on sets, nodes, and edges to exploring the tensor equivariance inherent in mappings. This allows for a more fundamental investigation of network design principles, enabling compatibility with both data-driven and model-driven methods, as well as supervised and unsupervised learning strategies.
- **Module Design:** Building on the mathematical foundations of TE, we design plug-and-play modules for each property. For multidimensional and high-order equivariance, we derived and provided equivalent models to existing methods, significantly simplifying deployment and enhancing scalability. For these modules, we further propose a approach that effectively decreases complexity while maintaining the network's ability to capture features across multiple dimensions. To model the invariance of the mapping across multiple dimensions, we constructed a multidimensional invariant module based on a Transformer-based layer.
- **Case Study & Experimental Validation:** By integrating TE with the proposed plug-and-play modules, we streamline the design of TE networks in addressing various MU-MIMO tasks. Based on the proposed framework, we focus on precoding and user scheduling, both typical tasks in MU-MIMO transmission, as study cases. We not only design the corresponding networks, but also perform extensive experimental validation. The simulation results demonstrate that the proposed framework exhibits advantages in terms of lower computational complexity, reduced parameter count, and good generalizability.

This paper is structured as follows: In Section II, we put forward TE in MU-MIMO systems. Section III proposes plug-and-play TENN modules. Section IV investigates the unified TE framework. Section V reports the simulation results, and the paper is concluded in Section VI.

Standard Notation: $(\cdot)^{-1}$, $(\cdot)^T$, $(\cdot)^H$ denote the inverse, transpose, and the transpose-conjugate operations, respectively. x , \mathbf{x} , \mathbf{X} , and \mathbf{X} respectively denote a scalar, column vector, matrix, and tensor. $\Re(\cdot)$ and $\Im(\cdot)$ represent the real and imaginary part of a complex scalars, vector or matrix. $j = \sqrt{-1}$ denote imaginary unit. \in denotes belonging to a set. $\mathcal{A} \setminus \mathcal{B}$ means objects that belong to set \mathcal{A} but not to \mathcal{B} . $|\mathcal{A}|$ represents the cardinality of set \mathcal{A} . \mathbf{I}_K denotes $K \times K$ identity matrix. $\mathbf{1}$ denotes the suitable-shape tensor with all

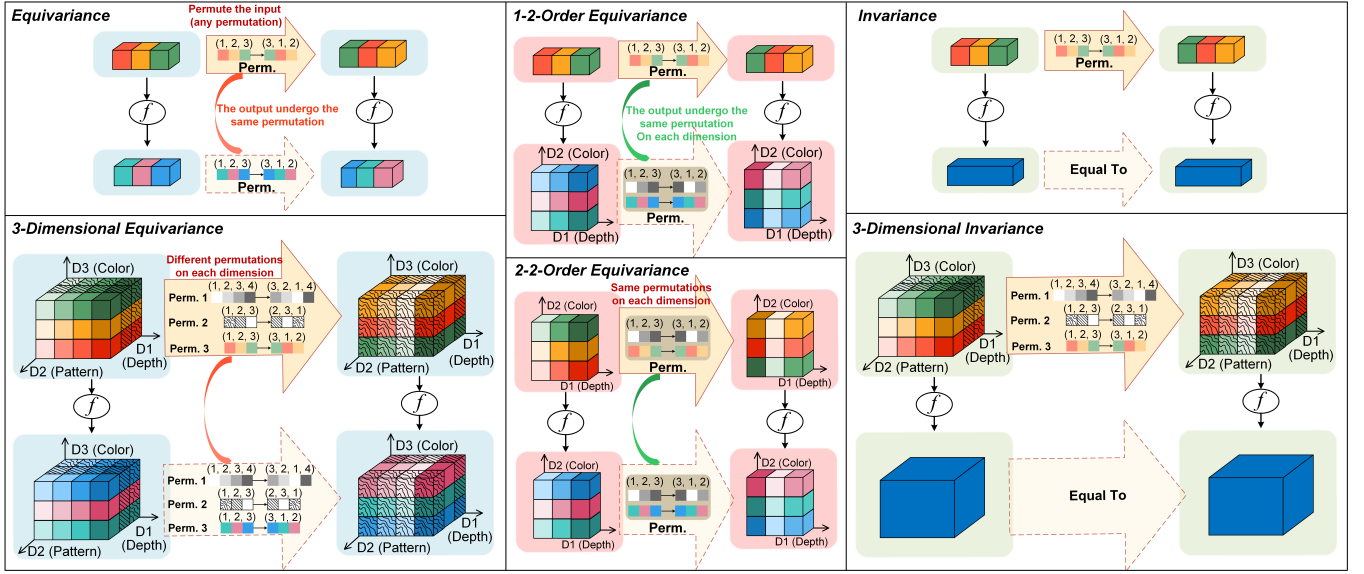


Fig. 1. Some examples of tensor equivariance. ‘Perm.’ denotes the abbreviation of permutation; depth, pattern, and color are used to distinguish different features across the three dimensions; the solid-bordered arrows represent performing a certain permutation on the tensor, while the dashed-bordered arrows denote the permutation relations satisfied between tensors.

elements being ones. $\|\cdot\|_2$ denotes l_2 -norm. $\det(\mathbf{A})$ represents the determinant of matrix \mathbf{A} . $\text{blkdiag}\{\mathbf{A}_1, \dots, \mathbf{A}_K\}$ represents a block diagonal matrix composed of $\mathbf{A}_1, \dots, \mathbf{A}_K$.

Tensor Notation: We use $\mathbf{X}_{[m_1, \dots, m_N]}$ to denote the indexing of elements in tensor $\mathbf{X} \in \mathbb{R}^{M_1 \times \dots \times M_N}$. $[\mathbf{A}_1, \dots, \mathbf{A}_K]_S$ denotes the tensor formed by stacking $\mathbf{A}_1, \dots, \mathbf{A}_K$ along the S -th dimension. $[\cdot]_0$ denotes the concatenation of tensors along a new dimension, i.e., $\mathbf{A}_{[n, \dots]} = \mathbf{B}_n, \forall n$ when $\mathbf{A} = [\mathbf{B}_1, \dots, \mathbf{B}_N]_0$. We define the product of tensor $\mathbf{X} \in \mathbb{R}^{M_1 \times \dots \times M_N \times D_X}$ and matrix $\mathbf{Y} \in \mathbb{R}^{D_X \times D_Y}$ as $(\mathbf{X} \times \mathbf{Y})_{[m_1, \dots, m_N, \cdot]} = \mathbf{X}_{[m_1, \dots, m_N, \cdot]} \mathbf{Y}$. The Kronecker product of tensor and matrix is defined as $(\mathbf{X} \otimes_n \mathbf{Y})_{[m_1, \dots, m_{n-1}, \cdot, \cdot, m_{n+2}, \dots, m_N]} = \mathbf{X}_{[m_1, \dots, m_{n-1}, \cdot, \cdot, m_{n+2}, \dots, m_N]} \otimes \mathbf{Y}$.

II. TENSOR EQUIVARIANCE IN MU-MIMO SYSTEMS

In this section, we first present the concept of TE, and then propose a research paradigm for exploiting inherent TE within mappings of communication problems.

A. Tensor Equivariance

Building on the properties in [41] and [44], we propose the mathematical definitions of multidimensional equivariance and high-order equivariance, which offer improved generality and simplicity. Additionally, we extend the permutation invariance from [28] to multidimensional invariance, which captures the permutation invariance exhibited by mappings across multiple dimensions. We unify the mathematical expressions of these three properties, collectively referred to as TE. Below, we will provide their specific definitions.

The *permutation* π_M denotes a shuffling operation on the index $[1, \dots, M]$ of a length- M vector under a specific pattern (or referred to as bijection from the indices set $\mathcal{M} = \{1, 2, \dots, M\}$ to \mathcal{M}), with the operator \circ denoting its operation, and $\pi_M(m)$ represents the result of mapping π_M on index m .

For example, if $\pi_3 \circ [x_1, x_2, x_3] = [x_2, x_3, x_1]$, then $\pi_3(1) = 2$, $\pi_3(2) = 3$, and $\pi_3(3) = 1$ [28]. For tensor, we further extend the symbol \circ to \circ_n , representing the permutation of dimension n in the tensor by π . For instance, if $\pi_3 \circ_2 \mathbf{X} = \mathbf{X}'$, then $\mathbf{X}_{[:,1,:]} = \mathbf{X}'_{[:,3,:]}$, $\mathbf{X}_{[:,2,:]} = \mathbf{X}'_{[:,1,:]}$, and $\mathbf{X}_{[:,3,:]} = \mathbf{X}'_{[:,2,:]}$. We define the *set of all permutations* for $[1, \dots, M]$ as \mathbb{S}_M , which is also referred to as the symmetric group [45], [46]. Then, we have $\pi_M \in \mathbb{S}_M$ and $|\mathbb{S}_M| = 2^M$.

Fig. 1 illustrates several properties encompassed by tensor equivariance in a diagrammatic form. Based on this, we will next introduce these properties.

The mapping $f : \mathbb{R}^{M_1 \times \dots \times M_N \times D_X} \rightarrow \mathbb{R}^{M_1 \times \dots \times M_N \times D_Y}$ exhibits *multidimensional (N -dimensional) equivariance* when it satisfies

$$f(\pi_{M_n} \circ_n \mathbf{X}) = \pi_{M_n} \circ_n f(\mathbf{X}), \forall \pi_{M_n} \in \mathbb{S}_{M_n}, \forall n \in \mathcal{N}. \quad (1)$$

where $\mathcal{N} = \{1, \dots, N\}$. This indicates that upon permuting a certain dimension in \mathcal{N} of the input, the order of items in the corresponding dimension of the output will also be permuted accordingly [11], [47], which aligns with those described in [41], [48].

We refer the mapping $f : \mathbb{R}^{\overbrace{M \times \dots \times M}^p \times D_X} \rightarrow \mathbb{R}^{\overbrace{M \times \dots \times M}^q \times D_Y}$ exhibits *high-order (p - q -order) equivariance* when it satisfies

$$f(\pi_M \circ_{[1, \dots, p]} \mathbf{X}) = \pi_M \circ_{[1, \dots, q]} f(\mathbf{X}), \forall \pi_M \in \mathbb{S}_M, \quad (2)$$

where $\pi_M \circ_{[1, \dots, p]}$ represents performing the same permutation π_M on the dimensions $1, \dots, p$, respectively. The above equation expresses the equivariance of the mapping f with respect to identical permutations across multiple dimensions, which originates from the descriptions in [42], [44]. We can distinguish between multidimensional and high-order equivariance by examining the permutation and the dimensions of

the input and output. Specifically, for a mapping with the same input and output dimensions as f in (2), it satisfies high-order equivariance whenever it satisfies multidimensional equivariance.

The mapping $f : \mathbb{R}^{M_1 \times \dots \times M_N \times D_X} \rightarrow \mathbb{R}^{D_Y}$ exhibits *multidimensional (N -dimensional) invariance* when it satisfies [43]

$$f(\pi_{M_n} \circ_n \mathbf{X}) = f(\mathbf{X}), \quad \forall \pi_{M_n} \in \mathbb{S}_{M_n}, \quad \forall n \in \mathcal{N}. \quad (3)$$

The above equation illustrates that permuting the indices of the input across the dimensions contained in \mathcal{N} does not affect the output of f . The properties described above are derived from the invariance in [28].

B. Tensor Equivariance in Precoding Design

In Sections II-B and II-C, we develop a research paradigm for exploiting TE, which first constructs the mapping between the available information and the optimal solution for the optimization problem, and then derives the TE that the mapping satisfies. As an example, we will validate the effectiveness of this paradigm for both data-driven and model-driven approaches in the precoding and user scheduling problems.

Consider an MU-MIMO system where a BS equipped with N_T antennas transmits signals to K users equipped with N_R antennas. The optimization problem of sum-rate maximization can be formulated as [19]:

$$\max_{\mathbf{W}} \sum_{k=1}^K R_k(\mathbf{H}, \mathbf{W}, \sigma^2) \quad \text{s.t.} \quad \sum_{k=1}^K \text{Tr}(\mathbf{W}_k \mathbf{W}_k^H) \leq P_T, \quad (4)$$

where $\mathbf{H} = [\mathbf{H}_1, \dots, \mathbf{H}_K]_0 \in \mathbb{C}^{K \times N_R \times N_T}$, $\mathbf{W} = [\mathbf{W}_1, \dots, \mathbf{W}_K]_0 \in \mathbb{C}^{K \times N_R \times N_T}$, $\mathbf{H}_k \in \mathbb{C}^{N_R \times N_T}$ denotes the channel from the BS to the k -th user, $\mathbf{W}_k \in \mathbb{C}^{N_R \times N_T}$ denotes the precoding matrix of the k -th user, P_T represents the fixed transmit power, σ^2 is the noise power, $R_k(\mathbf{H}, \mathbf{W}, \sigma^2) = \log \det(\mathbf{I}_k + \mathbf{W}_k \mathbf{H}_k^H \mathbf{\Omega}_k^{-1} \mathbf{H}_k \mathbf{W}_k^H)$ is the rate, and $\mathbf{\Omega}_k = \sigma^2 \mathbf{I} + \sum_{i=1, i \neq k}^K \mathbf{H}_i \mathbf{W}_i^H \mathbf{W}_i \mathbf{H}_i^H \in \mathbb{C}^{N_R \times N_R}$ is the effective Interference-plus-noise covariance matrix. It can be concluded that (4) is a problem for \mathbf{W} based on available CSI \mathbf{H} and σ^2 .

To simplify subsequent expressions, we define $\langle \mathbf{W}, \{\mathbf{H}, \sigma^2\} \rangle_P$ as a pairing of precoding and CSI for problem (4). Furthermore, the objective function achieved by \mathbf{W} and $\{\mathbf{H}, \sigma^2\}$ in problem (4) is denoted as “the objective function of $\langle \mathbf{W}, \{\mathbf{H}, \sigma^2\} \rangle_P$ ”. On this basis, the property of optimization problem (4) is as follows.

Proposition 1. *The objective function of $\langle \mathbf{W}, \{\mathbf{H}, \sigma^2\} \rangle_P$ is equal to those of $\langle \pi_K \circ_1 \mathbf{W}, \{\pi_K \circ_1 \mathbf{H}, \sigma^2\} \rangle_P$, $\langle \pi_{N_R} \circ_2 \mathbf{W}, \{\pi_{N_R} \circ_2 \mathbf{H}, \sigma^2\} \rangle_P$, and $\langle \pi_{N_T} \circ_3 \mathbf{W}, \{\pi_{N_T} \circ_3 \mathbf{H}, \sigma^2\} \rangle_P$, for all $\pi_K \in \mathbb{S}_K$, $\pi_{N_R} \in \mathbb{S}_{N_R}$, and $\pi_{N_T} \in \mathbb{S}_{N_T}$. Specifically, if $\langle \mathbf{W}^*, \{\mathbf{H}, \sigma^2\} \rangle_P$ achieves the optimal objective function, then $\langle \pi_K \circ_1 \mathbf{W}^*, \{\pi_K \circ_1 \mathbf{H}, \sigma^2\} \rangle_P$, $\langle \pi_{N_R} \circ_2 \mathbf{W}^*, \{\pi_{N_R} \circ_2 \mathbf{H}, \sigma^2\} \rangle_P$, and $\langle \pi_{N_T} \circ_3 \mathbf{W}^*, \{\pi_{N_T} \circ_3 \mathbf{H}, \sigma^2\} \rangle_P$ can also achieve their optimal objective functions.*

Proof. See Appendix A.

More clearly, we define $G_P(\cdot)$ as a mapping from available CSI to one of the optimal precoding schemes for (4), i.e.,

$G_P(\mathbf{H}, \sigma^2) = \mathbf{W}^*$. Then, based on **Proposition 1**, the following equations hold when problem (4) has a unique optimal solution.

$$G_P(\pi_K \circ_1 \mathbf{H}, \sigma^2) = \pi_K \circ_1 \mathbf{W}^*, \quad \forall \pi_K \in \mathbb{S}_K, \quad (5a)$$

$$G_P(\pi_{N_R} \circ_2 \mathbf{H}, \sigma^2) = \pi_{N_R} \circ_2 \mathbf{W}^*, \quad \forall \pi_{N_R} \in \mathbb{S}_{N_R}, \quad (5b)$$

$$G_P(\pi_{N_T} \circ_3 \mathbf{H}, \sigma^2) = \pi_{N_T} \circ_3 \mathbf{W}^*, \quad \forall \pi_{N_T} \in \mathbb{S}_{N_T}. \quad (5c)$$

If the optimization problem has multiple optimal solutions, it can be proven that the optimization problem based on the permuted CSI also has the same number of optimal solutions, and the optimal solutions of the two problems correspond one-to-one in the manner described by the equations above. In this case, $G_P(\cdot)$ can be regarded as a mapping to certain single optimal solution. To avoid potential performance degradation caused by the network fitting multiple mappings simultaneously, we can feed the initial solution as additional input to the network [26].

Then, we consider the TE in precoding design under the model-driven approach. For problem (4), iterative algorithms based on optimal closed-form expressions can achieve outstanding performance and have garnered considerable attention [4], [19]. The well-known solution to problem (4) can be obtained through the following expression [4]–[6]

$$\mathbf{W} = \gamma \tilde{\mathbf{W}}, \quad \tilde{\mathbf{W}} = \mathbf{H}^H \mathbf{A}^H \mathbf{U} (\mu \mathbf{I}_{M_K} + \mathbf{A} \mathbf{H} \mathbf{H}^H \mathbf{A}^H \mathbf{U})^{-1}, \quad (6)$$

$$\gamma = \sqrt{P_T / \text{Tr}(\tilde{\mathbf{W}} \tilde{\mathbf{W}}^H)}, \quad \mu = \text{Tr}(\mathbf{U} \mathbf{A} \mathbf{A}^H) \sigma^2 / P_T,$$

where

$$\mathbf{W} = [\mathbf{W}_1, \dots, \mathbf{W}_K]^T \in \mathbb{C}^{N_T \times K N_R}, \quad (7)$$

$$\mathbf{U} = \text{blkdiag}\{\mathbf{U}_1, \dots, \mathbf{U}_K\} \in \mathbb{C}^{K N_R \times K N_R}, \quad (8)$$

$$\mathbf{A} = \text{blkdiag}\{\mathbf{A}_1, \dots, \mathbf{A}_K\} \in \mathbb{C}^{K N_R \times K N_R}, \quad (9)$$

$$\mathbf{H} = [\mathbf{H}_1^T, \dots, \mathbf{H}_K^T]^T \in \mathbb{C}^{K N_R \times N_T}, \quad (10)$$

where $\mathbf{U}_k \in \mathbb{C}^{N_R \times N_R}$ and the Hermitian matrix $\mathbf{A}_k \in \mathbb{C}^{N_R \times N_R}$ are auxiliary tensors that require iterative computations with relatively high computational complexity to obtain based on $\{\mathbf{H}, \sigma^2\}$ [4]. To simplify the expression, we represent the aforementioned closed-form computation as $\mathbf{W} = \text{CFP}(\mathbf{H}, \mathbf{A}, \mathbf{U}, \sigma^2)$, where $\mathbf{A} = [\mathbf{A}_1, \dots, \mathbf{A}_K]_0 \in \mathbb{C}^{K \times N_R \times N_R}$ and $\mathbf{U} = [\mathbf{U}_1, \dots, \mathbf{U}_K]_0 \in \mathbb{C}^{K \times N_R \times N_R}$.

We define $\langle \{\mathbf{A}, \mathbf{U}\}, \{\mathbf{H}, \sigma^2\} \rangle_{\text{CFP}}$ as a pairing of auxiliary tensors and CSI for the closed-form expression to problem (4). The objective function achieved by $\mathbf{W} = \text{CFP}(\mathbf{H}, \mathbf{A}, \mathbf{U}, \sigma^2)$ and $\{\mathbf{H}, \sigma^2\}$ in problem (4) is denoted by “the objective function of $\langle \{\mathbf{A}, \mathbf{U}\}, \{\mathbf{H}, \sigma^2\} \rangle_{\text{CFP}}$ ”.

Proposition 2. *The objective function of $\langle \{\mathbf{A}, \mathbf{U}\}, \{\mathbf{H}, \sigma^2\} \rangle_{\text{CFP}}$ is equal to those of $\langle \{\pi_K \circ_1 \mathbf{A}, \pi_K \circ_1 \mathbf{U}\}, \{\pi_K \circ_1 \mathbf{H}, \sigma^2\} \rangle_{\text{CFP}}$, $\langle \{\pi_{N_R} \circ_{[2,3]} \mathbf{A}, \pi_{N_R} \circ_{[2,3]} \mathbf{U}\}, \{\pi_{N_R} \circ_2 \mathbf{H}, \sigma^2\} \rangle_{\text{CFP}}$, and $\langle \{\mathbf{A}, \mathbf{U}\}, \{\pi_{N_T} \circ_3 \mathbf{H}, \sigma^2\} \rangle_{\text{CFP}}$, for all $\pi_K \in \mathbb{S}_K$, $\pi_{N_R} \in \mathbb{S}_{N_R}$, and $\pi_{N_T} \in \mathbb{S}_{N_T}$. Specifically, if $\langle \{\mathbf{A}, \mathbf{U}\}, \{\mathbf{H}, \sigma^2\} \rangle_{\text{CFP}}$ achieves the optimal objective function¹, then $\langle \{\pi_K \circ_1 \mathbf{A}^*, \pi_K \circ_1 \mathbf{U}^*\}, \{\pi_K \circ_1 \mathbf{H}, \sigma^2\} \rangle_{\text{CFP}}$, $\langle \{\pi_{N_R} \circ_{[2,3]} \mathbf{A}^*, \pi_{N_R} \circ_{[2,3]} \mathbf{U}^*\}, \{\pi_{N_R} \circ_2 \mathbf{H}, \sigma^2\} \rangle_{\text{CFP}}$, and*

¹The optimal objective function here refers to the maximum achievable objective function of the closed-form expression in (6).

$\langle \{\mathbf{A}^*, \mathbf{U}^*\}, \{\pi_{N_T} \circ_3 \mathbf{H}, \sigma^2\} \rangle_{\text{CFP}}$ can also achieve their optimal objective functions.

Proof. See Appendix B.

Similar to **Proposition 1**, we define $G_{\text{CFP}}(\cdot)$ as a mapping from available CSI to one pair of the optimal auxiliary tensors for the closed-form expression (6) of problem (4), i.e., $G_{\text{CFP}}(\mathbf{H}, \sigma^2) = \mathbf{A}^*, \mathbf{U}^*$. When problem (4)'s closed-form (6) has only one pair of optimal auxiliary tensors, for all π_K , π_{N_R} , and π_{N_T} belonging to \mathbb{S}_K , \mathbb{S}_{N_R} , and \mathbb{S}_{N_T} , respectively, the following equations hold based on **Proposition 2**.

$$G_{\text{CFP}}(\pi_K \circ_1 \mathbf{H}, \sigma^2) = \pi_K \circ_1 \mathbf{A}^*, \pi_K \circ_1 \mathbf{U}^*, \quad (11a)$$

$$G_{\text{CFP}}(\pi_{N_R} \circ_2 \mathbf{H}, \sigma^2) = \pi_{N_R} \circ_{[2,3]} \mathbf{A}^*, \pi_{N_R} \circ_{[2,3]} \mathbf{U}^*, \quad (11b)$$

$$G_{\text{CFP}}(\pi_{N_T} \circ_3 \mathbf{H}, \sigma^2) = \mathbf{A}^*, \mathbf{U}^*. \quad (11c)$$

Furthermore, for MU-MISO system, the closed-form expression in (6) will degenerate to the closed-form expression in [19]. Except for the aspects related to the permutation of receive antennas, the remaining content in **Proposition 2** remains valid. Similar properties are also applicable to the preprocessed CSI and the modified precoding closed-form in [49].

C. Tensor Equivariance in User Scheduling Design

In this subsection, we consider the design of downlink user scheduling for the system in Section II-B, where K users are selected from \tilde{K} candidate users for downlink transmission, and the K users utilize a certain precoding scheme $\mathbf{W} = G_{\text{CP}}(\mathbf{H}, \sigma^2)$ for the downlink transmission. Without loss of generality, we assume that $G_{\text{CP}}(\cdot)$ possesses the properties described by (5a)-(5c). The user scheduling problem for sum-rate maximization is given by

$$\begin{aligned} \max_{\boldsymbol{\eta}} \quad & R_{\text{US}}(\tilde{\mathbf{H}}, \boldsymbol{\eta}, \sigma^2) \\ \text{s.t.} \quad & \eta_{\tilde{k}} \in \{0, 1\}, \tilde{k} \in \tilde{\mathcal{K}}, \\ & \sum_{\tilde{k} \in \tilde{\mathcal{K}}} \eta_{\tilde{k}} = K, \end{aligned} \quad (12)$$

where

$$R_{\text{US}}(\tilde{\mathbf{H}}, \boldsymbol{\eta}, \sigma^2) = \sum_{k \in \mathcal{K}} R_k(\mathbf{H}, G_{\text{CP}}(\mathbf{H}, \sigma^2), \sigma^2), \quad (13)$$

$$\mathcal{K} = \{k | \eta_k = 1, k \in \tilde{\mathcal{K}}\}, \tilde{\mathbf{H}} = [\mathbf{H}_k]_{0, k \in \tilde{\mathcal{K}}} \in \mathbb{C}^{\tilde{K} \times N_R \times N_T}, \quad (14)$$

$\eta_{\tilde{k}}$ is the scheduling indicator for user \tilde{k} , and $\boldsymbol{\eta} = [\eta_1, \dots, \eta_{\tilde{K}}]^T \in \mathbb{C}^{\tilde{K} \times 1}$. (12) is a problem for $\boldsymbol{\eta}$ based on $\tilde{\mathbf{H}}$ and σ^2 .

Similar to Section II-B, we define $\langle \boldsymbol{\eta}, \{\tilde{\mathbf{H}}, \sigma^2\} \rangle_{\text{US}}$ for problem (12), and the property of this problem is as follows.

Proposition 3. *The objective function of $\langle \boldsymbol{\eta}, \{\tilde{\mathbf{H}}, \sigma^2\} \rangle_{\text{US}}$ is equal to those of $\langle \pi_{\tilde{K}} \circ_1 \boldsymbol{\eta}, \{\pi_{\tilde{K}} \circ_1 \tilde{\mathbf{H}}, \sigma^2\} \rangle_{\text{US}}$, $\langle \boldsymbol{\eta}, \{\pi_{N_R} \circ_2 \tilde{\mathbf{H}}, \sigma^2\} \rangle_{\text{US}}$, and $\langle \boldsymbol{\eta}, \{\pi_{N_T} \circ_3 \mathbf{H}, \sigma^2\} \rangle_{\text{US}}$, for all $\pi_{\tilde{K}} \in \mathbb{S}_{\tilde{K}}$, $\pi_{N_R} \in \mathbb{S}_{N_R}$, and $\pi_{N_T} \in \mathbb{S}_{N_T}$. Furthermore, if $\langle \boldsymbol{\eta}^*, \{\tilde{\mathbf{H}}, \sigma^2\} \rangle_{\text{US}}$ achieves the optimal objective function, then $\langle \pi_{\tilde{K}} \circ_1 \boldsymbol{\eta}^*, \{\pi_{\tilde{K}} \circ_1 \tilde{\mathbf{H}}, \sigma^2\} \rangle_{\text{US}}$, $\langle \boldsymbol{\eta}^*, \{\pi_{N_R} \circ_2 \mathbf{H}, \sigma^2\} \rangle_{\text{US}}$, and $\langle \boldsymbol{\eta}^*, \{\pi_{N_T} \circ_3 \mathbf{H}, \sigma^2\} \rangle_{\text{US}}$ can also achieve their optimal objective functions.*

Proof. See Appendix C.

We define $G_{\text{US}}(\cdot)$ as a mapping from available CSI to one of the optimal binary selection variables for (12), i.e., $G_{\text{US}}(\tilde{\mathbf{H}}, \sigma^2) = \boldsymbol{\eta}^*$. Then, based on **Proposition 3**, the following equations hold when problem (12) has a unique optimal solution.

$$G_{\text{US}}(\pi_{\tilde{K}} \circ_1 \tilde{\mathbf{H}}, \sigma^2) = \pi_{\tilde{K}} \circ_1 \boldsymbol{\eta}^*, \forall \pi_{\tilde{K}} \in \mathbb{S}_{\tilde{K}}, \quad (15a)$$

$$G_{\text{US}}(\pi_{N_R} \circ_2 \tilde{\mathbf{H}}, \sigma^2) = \boldsymbol{\eta}^*, \forall \pi_{N_R} \in \mathbb{S}_{N_R}, \quad (15b)$$

$$G_{\text{US}}(\pi_{N_T} \circ_3 \tilde{\mathbf{H}}, \sigma^2) = \boldsymbol{\eta}^*, \forall \pi_{N_T} \in \mathbb{S}_{N_T}. \quad (15c)$$

III. TENSOR EQUIVARIANCE NN MODULES

In the previous section, we revealed the multidimensional equivariance (such as (5a)-(5c)), high-order equivariance (such as (11b)), and invariance (such as (11c), (15b), and (15c)) in the mappings required for MU-MIMO systems. In this section, we develop plug-and-play TENN modules that satisfy these properties, thereby laying the groundwork for constructing NNs for approximating mappings in MU-MIMO systems.

A. Multi-Dimensional Equivariant Module

In this subsection, we investigate function satisfying multidimensional equivariance to approximate the mapping like those in (5a)-(5c). The conventional FC layer processing involves flattening the features, multiplying them with a weight matrix, and adding bias. The operation $\text{FC}(\cdot) : \mathbb{R}^{M_1 \times \dots \times M_N \times D_I} \rightarrow \mathbb{R}^{M_1 \times \dots \times M_N \times D_O}$ can be represented as follows

$$\mathbf{Y} = \text{FC}(\mathbf{X}) = \text{vec}^{-1}(\mathbf{W} \text{vec}(\mathbf{X}) + \mathbf{b}), \quad (16)$$

where $\mathbf{X} \in \mathbb{R}^{M_1 \times \dots \times M_N \times D_I}$ denotes the input, $\mathbf{Y} \in \mathbb{R}^{M_1 \times \dots \times M_N \times D_O}$ represents the output, $\mathbf{W} \in \mathbb{R}^{\bar{M} D_I \times \bar{M} D_O}$ denotes the weight, $\mathbf{b} \in \mathbb{R}^{\bar{M} D_O \times 1}$ denotes the bias, and $\bar{M} = \prod_{n=1}^N M_n$. We refer D_I and D_O as the feature lengths.

The necessary and sufficient expressions of \mathbf{W} in layer $\mathbf{Y} = \text{vec}^{-1}(\mathbf{W} \text{vec}(\mathbf{X}))$ with N -dimensional equivariance is demonstrated in [41]. However, the intricate patterns of \mathbf{W} make its construction and deployment challenging, and it becomes increasingly difficult as the dimensionality increases. To this end, we derive a new equivalent mathematical expression that involves only simple operations, such as averaging across dimensions, making it easy to implement. Furthermore, we also consider the derivation of the patterns of \mathbf{b} . Based on this, we propose a method to significantly reduce the complexity of this module while maintaining nearly the same performance.

Firstly, to simplify subsequent expressions, we define $\tilde{\mathbf{X}}_{\mathcal{P}}$ to represent the result of averaging \mathbf{X} along the dimensions in \mathcal{P} and then repeating it to the original dimensions. Note that $\tilde{\mathbf{X}}_{\emptyset} = \mathbf{X}$. Besides, we denote $\tilde{\mathcal{N}}$ as the set containing all subsets of $\mathcal{N} = \{1, \dots, N\}$ (power set). As an example, when $N = 3$, Fig. 2 illustrates the acquisition of all $\tilde{\mathbf{X}}_{\mathcal{P}}$, $\mathcal{P} \in \tilde{\mathcal{N}}$.

Proposition 4. *Any FC layer $\mathbf{Y} = \text{FC}(\mathbf{X})$ satisfying multi-dimensional equivariance across dimensions M_1, M_2, \dots, M_N can be represented as*

$$\text{FC}_{\text{MDE}}(\mathbf{X}) = \sum_{\mathcal{P} \in \tilde{\mathcal{N}}} (\tilde{\mathbf{X}}_{\mathcal{P}} \times \mathbf{W}_{\mathcal{P}}) + \mathbf{1}_{\otimes N} \mathbf{b}_{\text{MDE}}^T, \quad (17)$$

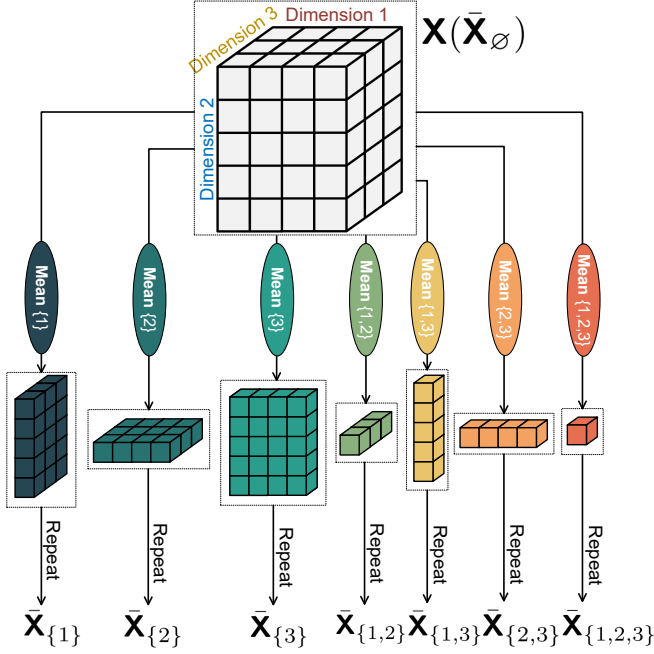


Fig. 2. In the case of $N = 3$, the acquisition for all $\tilde{\mathbf{X}}_{\mathcal{P}}$, $\mathcal{P} \subseteq \mathcal{N}$.

where $\mathbf{W}_{\mathcal{P}} \in \mathbb{R}^{D_1 \times D_0}$, $\forall \mathcal{P} \in \tilde{\mathcal{N}}$ and $\mathbf{b}_{\text{MDE}} \in \mathbb{R}^{D_0 \times 1}$ are learnable parameters.

Proof. See Appendix D.

Proposition 4 indicates that when equivariance is satisfied across N dimensions, the processing of the FC layer degenerates into linear combination of the means of the input tensor at all dimension combinations in \mathcal{N} . By defining $\text{FFC}(\cdot)$ as the learnable FC layer that applied to the last dimension, i.e., $\text{FFC}(\mathbf{X}) = \mathbf{X} \times \mathbf{W} + \mathbf{1}_{\otimes N} \mathbf{b}$, the layer in (17) can be achieved by $\text{FC}_{\text{MDE}}(\mathbf{X}) = \text{FFC}([\tilde{\mathbf{X}}_{\mathcal{P}}]_{N+1, \mathcal{P} \in \tilde{\mathcal{N}}})$.

Furthermore, we analyze the changes in computational complexity and the number of parameters brought about by this degeneration. In (16), for $\text{FC}(\cdot)$, the number of multiplications is $\mathcal{O}(\bar{M}^2 D_1 D_0)$, and the number of parameters is $\mathcal{O}(\bar{M}^2 D_1 D_0)$. For $\text{FC}_{\text{MDE}}(\cdot)$, since the power set of \mathcal{N} consists of 2^N elements, the computational complexity and the number of parameters are $\mathcal{O}(2^N \bar{M} D_1 D_0)$ and $\mathcal{O}(2^N D_1 D_0)$, respectively. Given $\bar{M} = \prod_{n=1}^N M_n$, it holds that $\bar{M} \gg 2^N$ when $M_n > 2, n \in \mathcal{N}$, which means $\text{FC}_{\text{MDE}}(\cdot)$ significantly reduces the complexity. Note that the computational complexity of $\text{FC}(\cdot)$ is determined by \bar{M}^2 , while that of $\text{FC}_{\text{MDE}}(\cdot)$ is only determined by \bar{M} . Furthermore, the number of parameters in $\text{FC}(\cdot)$ is dependent on \bar{M} , while that of $\text{FC}_{\text{MDE}}(\cdot)$ is solely determined by N .

The computational complexity and parameter count of the module are related to N by the relationship $\mathcal{O}(|\tilde{\mathcal{N}}|) = \mathcal{O}(2^N)$, and the complexity becomes high when N is large. To this end, we propose the approach to reduce the complexity, whose main idea is to replace the set $\tilde{\mathcal{N}}$ by its special subset $\tilde{\mathcal{N}}'$. $\tilde{\mathbf{X}}_{\mathcal{P}}$ represents one-dimensional and cross-dimensional global features in the case of $|\mathcal{P}| = 1$ and $|\mathcal{P}| > 1$, respectively. For a single-layer network, if we remove certain \mathcal{P} from the set $\tilde{\mathcal{N}}$ (where $\mathcal{P} \neq \emptyset$), the network will lose the ability

to capture global features in those dimension combinations. However, for a multi-layer network, even if some \mathcal{P} are removed, the network may still retain the capability to capture global features of various dimensional combinations through multi-layer stacking, similar to the receptive field mechanism in CNN [50]. Based on this, we propose the following three patterns for constructing set $\tilde{\mathcal{N}}'$, where $\tilde{\mathcal{N}}'_l$ represents the set of the l -th layer.

- **Pattern 1:** The set $\tilde{\mathcal{N}}'_l$ for each layer of the network is the same, which is

$$\tilde{\mathcal{N}}_l^{\text{P1}} = \{\emptyset, \{1\}, \{2\}, \dots, \{N\}\}, \forall l. \quad (18)$$

When $N = 3$, we have $\tilde{\mathcal{N}}_l^{\text{P1}} = \{\emptyset, \{1\}, \{2\}, \{3\}\}$. The complexity order is reduced from $\mathcal{O}(2^N)$ to $\mathcal{O}(N + 1)$.

- **Pattern 2:** The set $\tilde{\mathcal{N}}'_l$ for each layer of the network can be different, but must include the empty set \emptyset . The included sets must satisfy $|\mathcal{P}| \leq 1$ and need to satisfy

$$\tilde{\mathcal{N}}_1^{\text{P2}} \cup \tilde{\mathcal{N}}_2^{\text{P2}} \cup \dots \cup \tilde{\mathcal{N}}_L^{\text{P2}} = \{\emptyset, \{1\}, \dots, \{N\}\}. \quad (19)$$

For example, when $N = 3$ and $L = 3$, the sets can be $\tilde{\mathcal{N}}_1^{\text{P2}} = \{\emptyset, \{1\}, \{2\}\}$, $\tilde{\mathcal{N}}_2^{\text{P2}} = \{\emptyset, \{2\}, \{3\}\}$, and $\tilde{\mathcal{N}}_3^{\text{P2}} = \{\emptyset, \{1\}, \{3\}\}$. The above equation ensures that there is no loss of global feature for all dimensions throughout the entire network. The complexity order is reduced from $\mathcal{O}(2^N)$ to $\mathcal{O}(N')$, where $N' \leq N + 1$.

- **Pattern 3:** The sets $\tilde{\mathcal{N}}'_l$ of different layers can be different, but they only contain two elements, \emptyset and \mathcal{P}_l , where $|\mathcal{P}_l| = 1$, and they need to satisfy

$$\mathcal{P}_1 \cup \mathcal{P}_2 \cup \dots \cup \mathcal{P}_L = \{\{1\}, \dots, \{N\}\}. \quad (20)$$

For example, when $N = 3$ and $L = 3$, the sets can be $\tilde{\mathcal{N}}_1^{\text{P3}} = \{\emptyset, \{1\}\}$, $\tilde{\mathcal{N}}_2^{\text{P3}} = \{\emptyset, \{2\}\}$, and $\tilde{\mathcal{N}}_3^{\text{P3}} = \{\emptyset, \{3\}\}$. This pattern can be regarded as a special case of **Pattern 2**. The complexity order is reduced from $\mathcal{O}(2^N)$ to $\mathcal{O}(2)$.

B. High-Order Equivariant Module

In this subsection, we construct functions satisfying high-order equivariance. The necessary and sufficient parameter-sharing pattern for \mathbf{W} and \mathbf{b} in layer $\mathbf{Y} = \text{vec}^{-1}(\mathbf{W} \text{vec}(\mathbf{X}) + \mathbf{b})$ with p - q -order equivariance is demonstrated in [44], which describes the element-wise relationship between the output and input under complex set definitions. Based on this work, we propose a new mathematically equivalent model that is easier to understand, construct, and deploy.

Proposition 5. Any FC layer $\mathbf{Y} = \text{FC}(\mathbf{X})$ satisfying the p - q -order equivariance can be represented as

$$\text{FC}_{\text{HOE}}(\mathbf{X}) = \sum_{\mathcal{P} \in \tilde{\mathcal{N}}_{p-q}} (\tilde{\mathbf{X}}_{\mathcal{P}} \times \mathbf{W}_{\mathcal{P}}) + \sum_{\mathcal{Q} \in \tilde{\mathcal{N}}_q} \mathbf{B}_{\mathcal{Q}} \quad (21)$$

where $\mathbf{W}_{\mathcal{P}} \in \mathbb{R}^{D_1 \times D_0}$ is the learnable matrix for $\tilde{\mathbf{X}}_{\mathcal{P}}$, and $\mathbf{B}_{\mathcal{Q}}$ denotes the bias constructed based on set \mathcal{Q} . $\tilde{\mathbf{X}}_{\mathcal{P}}$ represents the output tensor formed by the simple combination of elements from the input tensor based on set \mathcal{P} . The construction of $\tilde{\mathcal{N}}$, $\tilde{\mathbf{X}}_{\mathcal{P}}$, and $\mathbf{B}_{\mathcal{Q}}$ can be found in Appendix E.

The proposition can be proved based on [44] and [51]. Similar to $\text{FC}_{\text{MDE}}(\cdot)$, $\text{FC}_{\text{HOE}}(\cdot)$ essentially performs a linear combination of the matrices constructed by input itself and its global feature across each dimension and their combinations. The computational complexity and parameter count of $\text{FC}(\cdot)$ are both $\mathcal{O}(M^{p+q}D_I D_O)$, while those of $\text{FC}_{\text{HOE}}(\cdot)$ are $\mathcal{O}(|\tilde{\mathcal{N}}_{p-q}|M^q D_I D_O)$ and $\mathcal{O}(D_I D_O)$, respectively. Note that $|\tilde{\mathcal{N}}_{p-q}| = B(p+q)$, where $B(\cdot)$ is the Bell number. Specifically, the construction details of the 1-2-order equivariant module are provided in Appendix E. When applied to tensors, one can only do the operation for certain two dimensions and regard the other dimensions as batch dimensions. For example, when we apply 1-2-order $\text{FC}_{\text{HOE}}(\cdot) : \mathbb{R}^{M \times D_I} \rightarrow \mathbb{R}^{M \times M \times D_O}$ to the last two dimensions of $\mathbf{X} \in \mathbb{R}^{M_1 \times \dots \times M_N \times D_I}$, for all $m_1 \in \{1, \dots, M_1\}, \dots, m_{N-1} \in \{1, \dots, M_{N-1}\}$, execute the following same operation

$$\mathbf{Y}_{[m_1, \dots, m_{N-1}, :, :, :]} = \text{FC}_{\text{HOE}}(\mathbf{X}_{[m_1, \dots, m_{N-1}, :, :, :]}) \in \mathbb{R}^{M_N \times M_N \times D_O}. \quad (22)$$

The above operation can be executed in parallel through batch computation.

It is worth noting that the mathematical expression of (21) is consistent with the multidimensional equivariant module (17), which means that we can adopt a similar approach by constructing subset $\tilde{\mathcal{N}}'_{p-q,l}$ to replace set $\tilde{\mathcal{N}}_{p-q}$, thereby significantly reducing the complexity. Specifically, when constructing a network by stacking multiple high-order equivariant modules, we can either remove all $\mathcal{P} \in \tilde{\mathcal{N}}_{p-q}$ containing features across multiple dimensions (Pattern 1); or, further refine each module by removing parts of the $\mathcal{P} \in \tilde{\mathcal{N}}_{p-q}$ that contain features within every single dimension (Pattern 2); or construct the set $\tilde{\mathcal{N}}'_{p-q,l}$ for each module by retaining only \mathcal{P} that keeps specific single-dimensional features (Pattern 3).

C. Multi-Dimensional Invariant Module

In this subsection, we first introduce function PMA in [43], which satisfies single-dimensional invariance. On this basis, we extend PMA and propose the multidimensional invariant module, which can capture the invariance of mappings across multiple dimensions.

The expression of PMA is as follows

$$\text{PMA}(\mathbf{X}) = \text{MAB}(\mathbf{S}, \text{FFC}(\mathbf{X})) \in \mathbb{R}^{J \times D_O}, \quad (23)$$

where $\mathbf{X} \in \mathbb{R}^{M \times D_I}$ is the input matrix, and $\mathbf{S} \in \mathbb{R}^{J \times D_I}$ is a learnable parameter matrix, M denotes the number of input items, and D_O represents the output feature length. J controls the dimension of the output matrix. Without loss of generality, we all subsequently set $J = 1$. The expression of $\text{MAB}(\cdot)$ is given by²

$$\text{MAB}(\mathbf{X}', \mathbf{Y}') = \mathbf{M}' + \text{ReLU}(\text{FFC}(\mathbf{M}')), \quad (24)$$

$$\mathbf{M}' = \text{LN}(\mathbf{X}' + \text{MultiHead}(\mathbf{X}', \mathbf{Y}', \mathbf{Y}')). \quad (25)$$

²The matrices in the expression are only used for illustrative purposes, so the matrix dimensions are not given.

$\text{MultiHead}(\cdot)$ denotes the multi-head attention module [52], whose expression can be written as $\text{MultiHead}(\mathbf{Q}, \mathbf{K}, \mathbf{V}) = [\text{head}_1, \dots, \text{head}_{N_H}] \mathbf{W}^O$, where

$$\text{head}_i = \text{Attention}(\mathbf{Q} \mathbf{W}_i^Q, \mathbf{K} \mathbf{W}_i^K, \mathbf{V} \mathbf{W}_i^V), \quad (26)$$

where $\mathbf{W}^Q, \mathbf{W}^K, \mathbf{W}^V \in \mathbb{R}^{D_I \times \frac{D_O}{N_H}}$ and $\mathbf{W}^O \in \mathbb{R}^{D_O \times D_O}$ are learnable weights; N_H is the number of heads. The $\text{Attention}(\cdot)$ function is given by

$$\text{Attention}(\bar{\mathbf{Q}}, \bar{\mathbf{K}}, \bar{\mathbf{V}}) = \text{Softmax}\left(\bar{\mathbf{Q}} \bar{\mathbf{K}}^T / \sqrt{D_I / N_H}\right) \bar{\mathbf{V}}, \quad (27)$$

where Softmax is performed at the second dimension. In summary, the process of $\text{PMA}(\cdot)$ are given by (23)-(27).

It is easy to prove that the parameterized invariant function $\text{PMA} : \mathbb{R}^{M \times D_I} \rightarrow \mathbb{R}^{1 \times D_O}$ satisfies the invariance. Similar to $\text{FC}_{\text{HOE}}(\cdot)$, $\text{PMA}(\cdot)$ can be applied to a certain dimension of a tensor with batch computation. The computational complexity of $\text{PMA}(\cdot)$ mainly resides in (24)-(27), denoted as $\mathcal{O}(M D_O (D_I + D_O))$, with the number of parameters $\mathcal{O}(D_O (D_I + D_O))$.

According to the definition of multidimensional invariance, we construct the module $\text{MDI}_{\mathcal{P}}(\cdot)$, which applies distinct PMA across each dimension in the set \mathcal{P} . For example, to model an invariant mapping $f : \mathbb{R}^{M_1 \times \dots \times M_N \times D_X} \rightarrow \mathbb{R}^{D_Y}$, let $\mathcal{P} = \mathcal{N}$, and its expression is given by

$$\text{MDI}_{\mathcal{P}}(\mathbf{X}) = [\text{PMA}_1 \circ_1 \dots \text{PMA}_N \circ_N \mathbf{X}], \quad (28)$$

where PMA_n refers to the n -th PMA module, \circ_n denotes the computation of PMA along the n -th dimension, and the brackets $[\cdot]$ indicate the removal of empty dimensions of size 1 generated during this process.

D. Advantages of TENN Modules

The TENN modules designed in Sections III-A-III-C satisfy TE that aligns with mappings mentioned in Section II. Considering conventional NNs can approximate almost any mapping [10], a natural question arises: *Why should we exploit TE for NN design?* Based on the analysis in Sections III-A-III-C, we provide several reasons as follows:

- **Parameter sharing:** The TENN modules lead to specific parameter sharing patterns [29], [41], greatly reducing the number of parameter. Furthermore, the parameter count is independent of input size, which provides advantages for scenarios that involve a large number of items [53].
- **Lower complexity:** Under the parameter-sharing pattern, the restructuring of network operations (e.g., the multidimensional equivariant module discussed in Section III-A) reduces the computational complexity of forward propagation. As the input size increases, the rate of complexity growth is relatively slow.
- **Flexible input size:** Since the parameters of equivariant networks are independent of the number of inputs, the network can work in scenarios with different input sizes without any modification [28], [44].
- **Widespread presence:** It is easily demonstrated that the design of modulation [54], soft demodulation [40], detection [39], channel estimation [55] (or other parameter

estimation), and other aspects also involve TE. Moreover, the dimensionality of these properties grows with the increases of device types in the system, such as access points, reconfigurable intelligent surfaces, and unmanned aerial vehicles.

IV. TENSOR EQUIVARIANCE FRAMEWORK FOR NN DESIGN

In this section, by leveraging the plug-and-play TENN modules, we first present the TE framework for NN design. Based on this framework, we construct NNs for solving optimization problems outlined in Sections II-B and III-B, respectively, as exemplified.

A. Unified TE Framework

Firstly, we present the following proposition to establish the foundation for stacking equivariant layers, thus achieving multidimensional equivariance, high-order equivariance, and invariance in certain dimensions.

Proposition 6. *The high-order equivariant layers and multidimensional invariant layers retain their properties when stacked with multidimensional equivariant layers in front of them.*

Proof. See Appendix F.

The above proposition applies not only to the proposed modules but also to any other AI module that satisfies the properties. Building upon this proposition, we propose the following design framework.

- 1) **Find TE:** Similar to Section II-B and Section II-C, formulate the optimization problem, construct the target mapping from the available information to the optimal solution, and then derive the TE that the target mapping possesses.
- 2) **Construct \mathbf{X} and \mathbf{Y} :** Given the properties to be satisfied in each dimension, available tensors are manipulated through operations such as repetition and concatenation to construct the input \mathbf{X} of the network. Similarly, the desired output \mathbf{Y} is constructed for the required tensors.
- 3) **Build equivariant network:** Based on the TE required by the mapping from \mathbf{X} to \mathbf{Y} , select modules from those proposed in Section II, and then stack them to form the equivariant NN.
- 4) **Design the output layer:** The schemes in wireless communication system are usually constrained by various limitations, such as the transmit power. Therefore, it is necessary to design the output layer of the network to ensure that the outputs satisfy the constraints.

It is noteworthy that most of the existing techniques applicable to the design of AI-assisted communication schemes remain relevant within this framework. For instance, the technique of finding low-dimensional variables in [18], the approach for non-convex optimization problems presented in [26], and the residual connection for deep NNs in [56].

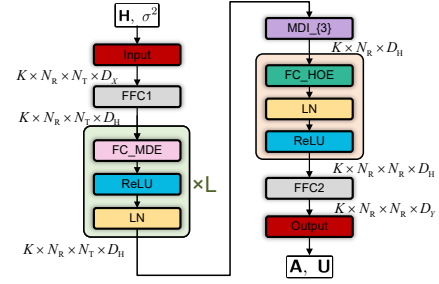


Fig. 3. The architecture of TEPN.

B. TENN Design for Precoding

Compared to the precoding tensor \mathbf{W} , the auxiliary tensors \mathbf{A}^* , \mathbf{U}^* in the optimal closed-form expression have smaller size, and incorporating such expression as the model-driven component can reduce the difficulty of NN training. Therefore, in this section, we consider designing NN to approximate the mapping from \mathbf{H}, σ^2 to $\mathbf{A}^*, \mathbf{U}^*$.

1) *Find TE:* According to Section II-B, the mapping satisfies the equivariance in (11a)-(11c).

2) *Construct the Input and Output:* We construct the input and output of the equivariant network as follows

$$\mathbf{X} = [\Re(\mathbf{H}), \Im(\mathbf{H}), \sigma^2 \mathbf{1}]_4 \in \mathbb{R}^{K \times N_R \times N_T \times D_X}, \quad (29)$$

$$\mathbf{Y} = [\Re(\mathbf{A}^*), \Im(\mathbf{A}^*), \Re(\mathbf{U}^*), \Im(\mathbf{U}^*)]_4 \in \mathbb{R}^{K \times N_R \times N_R \times D_Y}, \quad (30)$$

where $D_X = 3$ and $D_Y = 4$. The mapping $G(\cdot)$ from \mathbf{X} to \mathbf{Y} satisfies the following properties

$$G(\pi_K \circ_1 \mathbf{X}) = \pi_K \circ_1 \mathbf{Y}, \quad \forall \pi_K \in \mathbb{S}_K, \quad (31)$$

$$G(\pi_{N_R} \circ_2 \mathbf{X}) = \pi_{N_R} \circ_{[2,3]} \mathbf{Y}, \quad \forall \pi_{N_R} \in \mathbb{S}_{N_R}, \quad (32)$$

$$G(\pi_{N_T} \circ_3 \mathbf{X}) = \mathbf{Y}, \quad \forall \pi_{N_T} \in \mathbb{S}_{N_T}. \quad (33)$$

3) *Build Equivariant Network:* The constructed network is illustrated in Fig. 3. We first use the $\text{FFC}_1(\cdot)$ to elevate the feature length of \mathbf{X} from D_X to the hidden layer feature length D_H . Since the desired function $G(\cdot)$ exhibits equivariance in the first three dimensions of \mathbf{X} , we employ L multidimensional ($N = 3$) equivariant module $\text{FC}_{\text{MDE}}(\cdot)$ from Section III-A to perform the interaction between features of \mathbf{X} . Furthermore, considering the invariance of $G(\cdot)$ in (33), we employ the module $\text{MDI}_{\{3\}}(\cdot)$ from Section III-C, which satisfies the invariance, on the third dimension. Additionally, to satisfy the high-order equivariance in (32), we apply the high-order equivariant module $\text{FC}_{\text{HOE}}(\cdot)$ from Section III-B on the second dimension. D_I and D_O of all mentioned equivariant modules are equal to D_H . Finally, we employ $\text{FFC}_2(\cdot)$ to reduce the feature length from D_H to D_Y . Between modules, we incorporate ReLU for element-wise nonlinearity, and adopt layer normalization (LN) to expedite training and improve performance [57]. We refer to this network used for precoding as ‘TEPN’.

4) *Design the Output Layer:* \mathbf{A} and \mathbf{U} are key variables in the closed-form precoding expression, with constraints not explicitly shown. Therefore, the operations at the output layer

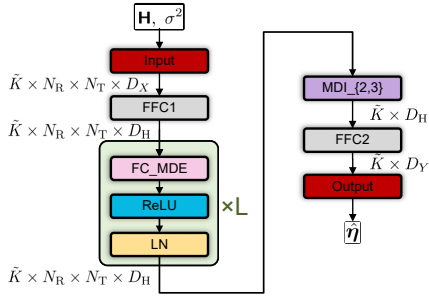


Fig. 4. The architecture of TEUSN.

are as follows

$$\mathbf{A} = \mathbf{Y}_{[:, :, :, 1]} + j\mathbf{Y}_{[:, :, :, 2]}, \quad \mathbf{U} = \mathbf{Y}_{[:, :, :, 3]} + j\mathbf{Y}_{[:, :, :, 4]}. \quad (34)$$

By combining the decomposition of tensors into matrices and the concatenation of matrices into tensors, we can compute the final precoding scheme $\hat{\mathbf{W}}$ from \mathbf{A} and \mathbf{U} using (6).

Given the optimization problem (4) for precoding, we employ unsupervised learning, with the negative loss function chosen as the objective function of problem (4), i.e.,

$$\text{Loss} = -\frac{1}{1/N_{\text{sp}}} \sum_{n=1}^{N_{\text{sp}}} \sum_{k=1}^K R_k(\mathbf{H}[n], \hat{\mathbf{W}}[n], \sigma^2[n]), \quad (35)$$

where the subscript $[n]$ denotes the n -th sample in the dataset, and N_{sp} represents the number of samples.

C. TENN Design for User Scheduling

1) *Find TE*: According to Section II-B, the design of the user scheduling scheme targets to find the mapping from $\tilde{\mathbf{H}}, \sigma^2$ to $\boldsymbol{\eta}^*$, which satisfies the equivariance in (15a)-(15c).

2) *Construct the Input and Output*: We construct the input and output as follows

$$\mathbf{X} = [\Re(\tilde{\mathbf{H}}), \Im(\tilde{\mathbf{H}}), \sigma^2 \mathbf{1}]_4, \quad \mathbf{y} = \boldsymbol{\eta}^*. \quad (36)$$

The mapping $G(\cdot)$ from \mathbf{X} to \mathbf{y} satisfies the following properties

$$G(\pi_{\tilde{K}} \circ_1 \mathbf{X}) = \pi_{\tilde{K}} \circ_1 \mathbf{y}, \quad \forall \pi_{\tilde{K}} \in \mathbb{S}_{\tilde{K}}, \quad (37)$$

$$G(\pi_{N_R} \circ_2 \mathbf{X}) = \mathbf{y}, \quad \forall \pi_{N_R} \in \mathbb{S}_{N_R}, \quad (38)$$

$$G(\pi_{N_T} \circ_3 \mathbf{X}) = \mathbf{y}, \quad \forall \pi_{N_T} \in \mathbb{S}_{N_T}. \quad (39)$$

3) *Build Equivariant Network*: The constructed network is illustrated in Fig. 4. The overall structure is similar to TEPN. The difference lies in replacing $\text{FC}_{\text{HOE}}(\cdot)$ with another $\text{MDI}_{\{2,3\}}(\cdot)$ to satisfy invariance in the second and third dimensions. We refer to this network used for user scheduling as ‘TEUSN’.

4) *Design the Output Layer*: In problem (12), $\boldsymbol{\eta}$ is constrained as a binary variable with all elements summing up to K . To address this, we first employ $\text{Softmax}(\cdot)$ to transform the output \mathbf{Y} into probabilities between 0 and 1, i.e., $\boldsymbol{\eta}^{\text{pro}} = \text{Softmax}(\mathbf{y})$. Subsequently, the largest K elements are set to 1, while the rest are set to 0, which is further denoted by $\hat{\boldsymbol{\eta}}$.

We employ supervised learning, utilizing the following binary cross-entropy loss for training

$$\text{Loss} = -\frac{1}{N_{\text{sp}} \tilde{K}} \sum_{n=1}^{N_{\text{sp}}} \sum_{k=1}^{\tilde{K}} \text{BCE}(\boldsymbol{\eta}_k^{\text{pro}}[n], \boldsymbol{\eta}_k^*[n]), \quad (40)$$

where $\boldsymbol{\eta}^*$ is the target result, and $\text{BCE}(a, b) = a \log(b) + (1 - a) \log(1 - b)$.

V. NUMERICAL RESULTS

In this section, we employ the Monte Carlo method to assess the performance of the proposed methods. We consider a massive MIMO system and utilize QuaDRiGa channel simulator to generate all channel data [58]. The configuration details of the channel model are as follows: The BS is equipped with uniform planar array (UPA) comprising $N_{\text{Tv}} = 2$ dual-polarized antennas in each column and N_{Th} dual-polarized antennas in each row with the number of antennas $N_{\text{T}} = 2N_{\text{Tv}}N_{\text{Th}}$. UEs are equipped with uniform linear array comprising $N_{\text{Rv}} = 1$ antennas in each column and N_{Rh} antennas in each row with the number of antennas $N_{\text{R}} = N_{\text{Rv}}N_{\text{Rh}}$. In this section, parameters N_{Th} and N_{Rh} are adjusted to accommodate the desired antenna quantity configuration. Both the BS and UEs employ antenna type ‘3gpp-3d’, the center frequency is set at 3.5 GHz, and the scenario is ‘3GPP_38.901_UMa_NLOS’ [59]. Shadow fading and path loss are not considered. The cell radius is 500 meters, with users distributed within a 120-degree sector facing the UPA (3-sector cell). For the convenience of comparison, we consider the normalized channel satisfying $\sum_{k=1}^K \text{Tr}\{\mathbf{H}_k \mathbf{H}_k^H\} = KN_{\text{R}}N_{\text{T}}$ and $\text{SNR} = P_{\text{T}}/\sigma^2$ [60]. Under the same channel model configuration, all channel realizations are independently generated, implying diversity in the channel environments and terminal locations.

A. Training Details

For the network TEPN constructed for precoding in Section IV-B, its channel dataset size is $[60000, K, N_{\text{R}}, N_{\text{T}}, 2]$, with 55000 channels used for training and 5000 channels used for testing, and the channels are stored as real and imaginary parts. Similarly, for the network TEUSN constructed for user scheduling in Section IV-C, its channel dataset size is $[60000, \tilde{K}, N_{\text{R}}, N_{\text{T}}, 2]$. Besides the label ($\boldsymbol{\eta}^*$) dataset size is $[60000, \tilde{K}, 1]$, where $\boldsymbol{\eta}^*$ is generated by well-performing conventional scheduling algorithms, as will be discussed in subsequent sections. We employ the same training strategy for TEPN and TEUSN. The number of iterations and batch size are set to be 2×10^5 and 2000. We utilize the Adam optimizer with a learning rate of 5×10^{-4} for the first half of training and 5×10^{-5} for the latter half [61]. It should be noted that during training for TEPN, we provided data with noise under different SNR levels, randomly drawn from $\{0, 5, 10, 15, 20, 25, 30, 25, 40\}$. This enables the network to operate effectively across various SNRs, while achieving a good trade-off between performance and storage overhead. Similarly, data at SNRs $\{0, 10, 20, 30, 40\}$ are used for training TEUSN. Considering that the training of TEUSN requires labeled data, we can achieve a tradeoff between performance

TABLE I
COMPUTATIONAL COMPLEXITY OF PRECODING SCHEMES

Methods	Complexity Order	Multiplications
ZF	$\mathcal{O}(N_T K^2 N_R^2)$	6.1×10^4
MMSE	$\mathcal{O}(N_T K^2 N_R^2)$	6.1×10^4
WMMSE-RandInt	$\mathcal{O}(T_{P1} N_T K^2 N_R^2)$	3.0×10^7
WMMSE-MMSEInit	$\mathcal{O}(T_{P2} N_T K^2 N_R^2)$	3.1×10^7
GNN	$\mathcal{O}(N_T K N_R D_G^2)$	1.0×10^8
DNN	$\mathcal{O}(N_T K N_R D_D + D_D^2)$	8.5×10^5
CNN	$\mathcal{O}(N_T K N_R N_C^2 + N_T K^2 N_R^2 N_C)$	2.9×10^6
TECFP	$\mathcal{O}(N_T K N_R D_H^2 + N_T K^2 N_R^2)$	1.0×10^6

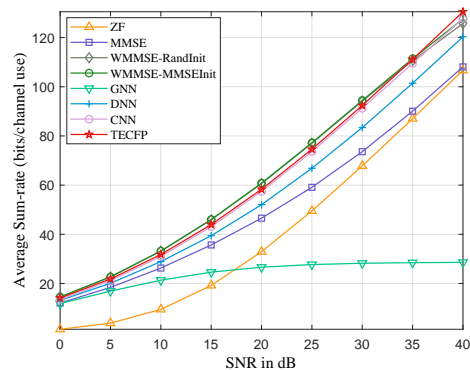
and training by reducing the diversity of SNR values and the number of channel samples in the dataset.

B. Performance of Precoding Schemes

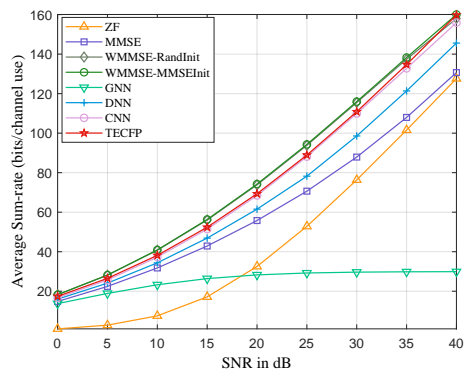
This section compares the following methods:

- ‘ZF’ and ‘MMSE’: Conventional closed-form linear precoding methods [62].
- ‘WMMSE-RandInt’ and ‘WMMSE-MMSEInit’: Conventional algorithms for iterative solving of the sum-rate maximization precoding problem [4]. ‘-RandInt’ and ‘-MMSEInit’ represent using random tensor and MMSE precoding as initial values, respectively. The maximum number of iterations is set to 300 and the stopping criterion is defined as a reduction in the sum-rate per single iteration being less than 10^{-4} . Similar to most precoding studies, we adopt WMMSE as our state-of-the-art baseline.
- ‘GNN’: The AI-aided approach utilizing GNN for computation of precoding tensors from CSI [36], where the number of hidden layers is 4 and the number of hidden layer neurons is $D_G = 128$.
- ‘DNN’: The model-driven AI-aided precoding method based on fully-connected deep NN [13].
- ‘CNN’: The AI-aided precoding method utilizes the CNN network in [49] to obtain auxiliary variables in the optimal closed form of precoding.
- ‘TECFP’: The precoding scheme based TEPN in Section IV-B with $L = 3$ and $D_H = 8$.

Table I contrasts the computational complexities of several methods under scenario $N_T = 32, K = 8, N_R = 2$. “Multiplications” refers to the count of real multiplications, with complex multiplications calculated as three times the real ones. It is noteworthy that in the table, $D_D > T_{P1} \approx T_{P2} > D_G \gg N_T > K \approx D_H \approx N_C > N_R$, where D_D denotes the number of neurons in the hidden layers of the DNN, and N_C denotes the number of convolutional kernels in the CNN. Among the considered methods, the complexity of ZF and MMSE precoding, as closed-form linear precoding methods, is the lowest. Although the computational complexity per single iteration of WMMSE precoding shares the same order as MMSE, achieving optimal performance typically requires multiple iterations, introducing high complexity. GNN also exhibit weight-sharing properties, thus their complexity is solely related to the first order of the channel dimensions. However, due to the high dimensionality of the precoding tensor, the approximation for precoding computations requires

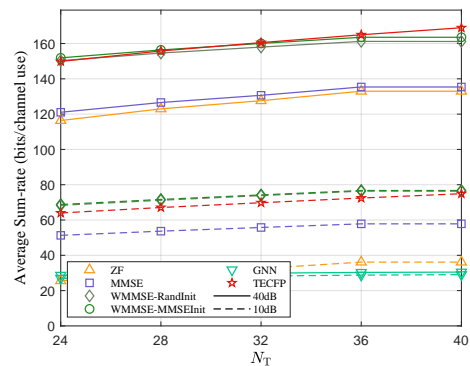


(a) $N_T = 24, K = 6$.

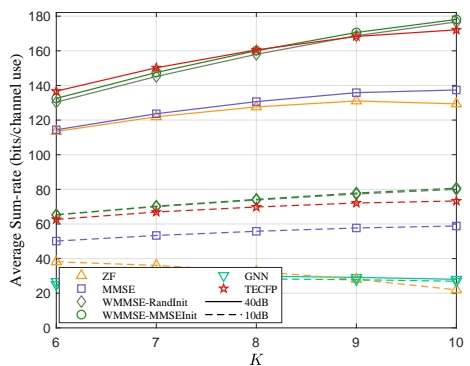


(b) $N_T = 32, K = 8$.

Fig. 5. Sum rate vs SNR, $N_R = 2$.

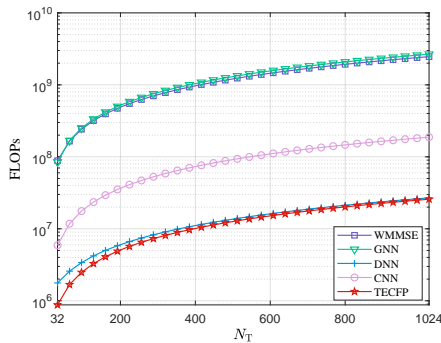
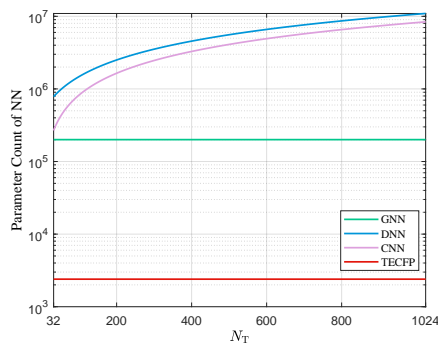
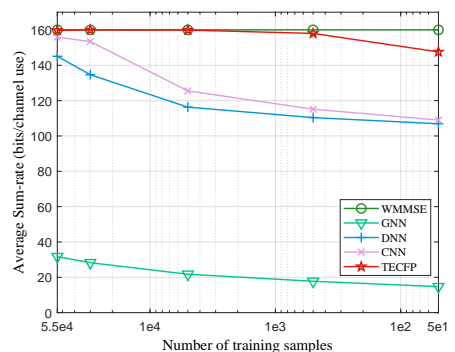


(a) Generalization for different N_T .



(b) Generalization for different K .

Fig. 6. Performance generalization of the network trained under scenario $N_T = 32, K = 8$, and $N_R = 2$.

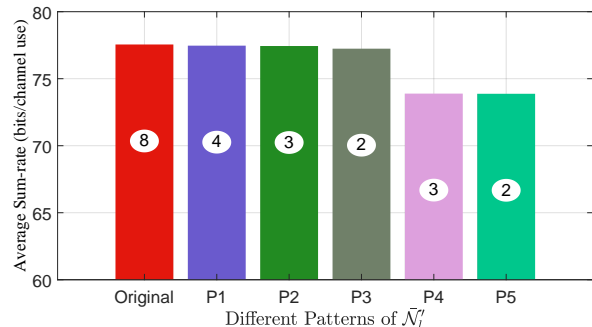
Fig. 7. FLOPs vs N_T , $K = 8$, $N_R = 2$.Fig. 8. Parameter counts vs N_T , $K = 8$, $N_R = 2$.Fig. 9. Performance vs training set size, $N_T = 32$, $K = 8$, $N_R = 2$, $\text{SNR} = 40\text{dB}$.

a substantial number of neurons D_G , thus introducing substantial complexity. TECFP leverages TE in mappings from CSI to auxiliary tensors, while enjoying the advantage of complexity being solely related to the first order of the channel size and requiring fewer neurons, thereby significantly reducing complexity. The required number of multiplications also validate the aforementioned analysis.

The comparison of sum-rate for each precoding scheme in scenarios $N_T = 32, K = 8, N_R = 2$ and $N_T = 24, K = 6, N_R = 2$ is illustrated in Fig. 5. It can be observed that the overall sum-rate performance of precoding schemes with lower computational complexity, such as ZF and MMSE, is significantly lower than that of WMMSE, validating the superior performance of WMMSE. Despite GNN employing a large number of parameters and computational complexity, their performance remains poor. This is attributed to the necessity of matrix inversion for high-dimensional matrices during the computation of precoding matrices [35]. In contrast, our proposed method integrates the advantages of model-driven approaches within the TE framework, enabling the approximation of WMMSE performance while maintaining low complexity. The performance of TECFP occasionally surpasses WMMSE at high SNR levels, possibly due to the heuristic nature of the WMMSE algorithm, which may result in suboptimal performance under high SNR conditions. Fig. 6 demonstrates the generalization capability of the proposed approach. We train our network in scenario $N_T = 32, K = 8, N_R = 2$ and directly apply it to various different scenarios. It can be observed that the proposed method exhibits consistently outstanding performance, highlighting its robust practical utility.

We compared the FLOPs with different N_T in Fig. 7. For different N_T , we only made necessary adjustments to the network architecture. Our method demonstrates lower FLOPs across various configurations, while its FLOP growth rate approaches that of DNN. The reason is that we did not adjust the number of neurons in the hidden layers of DNN. However, the performance of DNN is significantly influenced by the number of neurons in the hidden layers. Fig. 8 compares the changes in parameter count required by the NN to match input and output dimensions when the number of transmit antennas is adjusted. As the number of antennas increases, the FC layers in CNNs and DNNs require corresponding

adjustments, resulting in an increase in parameter count. In contrast, both our network and GNNs do not require any adjustments in parameter count, highlighting the advantages of the proposed method in handling large-scale problems. Fig. 9 compares the performance of the network when the training set contains different numbers of samples (\mathbf{H}). Without loss of generality, we maintain a consistent number of mini-batches across training on different dataset sizes. It can be observed that the performance of the proposed method declines at the slowest rate as dataset size decreases. This suggests that the proposed method requires a smaller dataset and has a stronger resistance to overfitting. This advantage stems from leveraging TE under the model-driven approach.

Fig. 10. Comparison of performance and complexity for multidimensional equivariance modules with different low-complexity patterns (set \mathcal{N}_l^l). The numbers on the bars represent the relative complexity.

Another interesting topic is the method proposed in Section III-A for further reducing the complexity of the multidimensional and high-order equivariant modules. For the multidimensional equivariance module, the main idea is constructing a subset \mathcal{N}_l^l to replace \mathcal{N} for the l -th layer of the network. In Section III-A, we provide three patterns with examples. The multidimensional equivariance module in the TECFP method is reconstructed according to these three examples, denoted as P1, P2, and P3. For comparison, we also present two additional patterns, P4: $\mathcal{N}_l^{P4} = \{\emptyset, \{1\}, \{3\}\}, \forall l$ and P5: $\mathcal{N}_l^{P5} = \{\emptyset, \{1\}\}, \forall l$. In Fig. 10 along with TECFP ('Original'), we compare the sum rate of these methods in the scenario $N_T = 32, K = 8, N_R = 2$, which is averaged over SNRs of $\{0, 5, \dots, 40\}$. In Fig. 10, the numbers on the bars

TABLE II
COMPUTATIONAL COMPLEXITY OF USER SCHEDULING SCHEMES

Methods	Complexity Order	Multiplications
MMSE-Rand	$\mathcal{O}(N_T K^2 N_R^2)$	6.1×10^4
MMSE-Greedy	$\mathcal{O}(K \tilde{K} (N_T K^2 N_R^2))$	1.8×10^6
MMSE-TEUS	$\mathcal{O}(N_T \tilde{K} N_R D_{H1}^2 + N_T K^2 N_R^2)$	1.4×10^6
WMMSE-Rand	$\mathcal{O}(T_{P2} N_T K^2 N_R^2)$	3.1×10^7
WMMSE-Greedy	$\mathcal{O}(K \tilde{K} (T_{P2} N_T K^2 N_R^2))$	6.4×10^8
WMMSE-TEUS	$\mathcal{O}(N_T \tilde{K} N_R D_{H2}^2 + T_{P2} N_T K^2 N_R^2)$	5.8×10^7
TECFP-TEUS	$\mathcal{O}(N_T \tilde{K} N_R D_{H2}^2 + N_T K^2 N_R^2)$	2.8×10^7

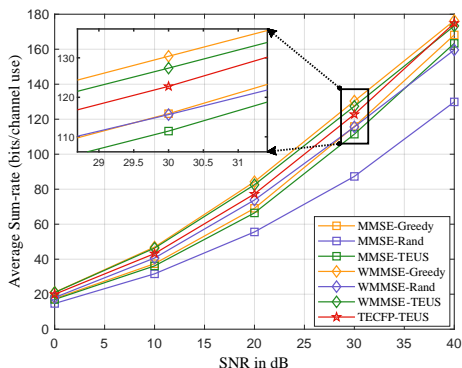


Fig. 11. Sum rate vs SNR, $N_T = 32$, $\tilde{K} = 12$, $K = 8$, $N_R = 2$.

represent the relative computational complexity and parameter counts of the modules under several patterns. For instance, under pattern P3, the computational complexity and parameter count of this module are 25% of those ('Original') in TECFP. It can be observed that the proposed patterns significantly reduce the complexity while ensuring good performance. In contrast, P4 and P5 do not satisfy (19), which results in a loss of the ability to capture global features across all dimensions, leading to a significant decline in performance.

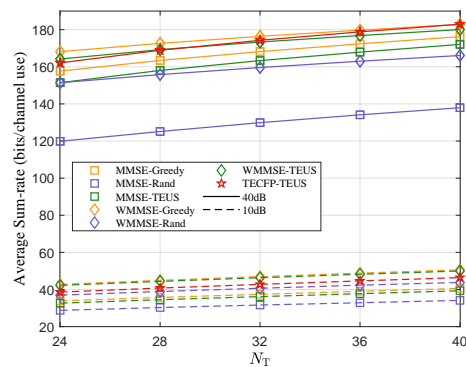
C. Performance of User Scheduling Schemes

Based on precoding schemes MMSE, WMMSE (MMSEInit), and TECFP as a foundation, we compare several user scheduling strategies as follows:

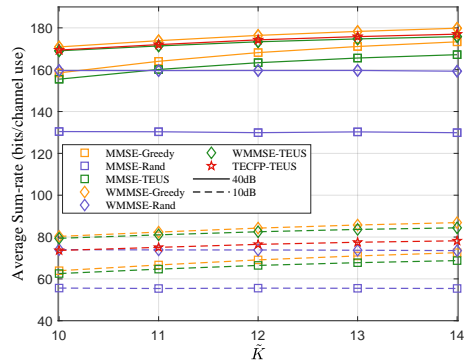
- **'Rand'**: Select K users randomly from \tilde{K} users.
- **'Greedy'**: Select users one by one from \tilde{K} users based on the criterion of maximizing the sum-rate after precoding for the selected users until reaching K users [3].
- **'TEUS'**: The scheduling strategy based on TEUSN trained with the result of greedy scheduling strategy as the label in Section IV-C.

The scheduling strategies vary among different precoding schemes. It is worth noting that the results of greedy user scheduling vary across different precoding schemes. The number of hidden layers and nodes in the TEUS used for MMSE and WMMSE are respectively denoted as $L = 3$, $D_H = 8$ and $L = 4$, $D_H = 32$.

We compare the computational complexity of several scheduling and precoding combination schemes in Table II under scenario $N_T = 32$, $\tilde{K} = 12$, $K = 8$, $N_R = 2$. It can be observed that although the greedy scheduling algorithm



(a) Generalization for different N_T .



(b) Generalization for different \tilde{K} .

Fig. 12. Performance generalization of the network trained under scenario $N_T = 32$, $\tilde{K} = 12$, $K = 8$, and $N_R = 2$.

is designed to select the near-optimal users, it introduces a high computational complexity. The proposed method, TEUS, significantly reduces the overall computational complexity of scheduling and precoding. Fig. 11 compares the sum-rate performance of various precoding and scheduling combination schemes under scenario $N_T = 32$, $\tilde{K} = 12$, $K = 8$, $N_R = 2$. It can be observed that the performance of MMSE-TEUS and WMMSE-TEUS is close to that of MMSE-Greedy and WMMSE-Greedy, respectively. This indicates that the proposed TEUS can achieve outstanding performance at lower computational complexity. Although the performance of TECFP-TEUS is slightly inferior to that of the proposed WMMSE-TEUS, its computational complexity is much lower, requiring less than 5% of that of WMMSE-Greedy. Furthermore, in Fig. 12, we compare the generalization ability of the proposed method across different scenarios. It is evident that, as the scenario changes, the performance trends of MMSE-TEUS, WMMSE-TEUS, and TECFP-TEUS are similar to those of the conventional algorithms MMSE-Greedy and WMMSE-Greedy. This implies that these proposed schemes possess outstanding capability to be directly extended for application in different scenarios.

VI. CONCLUSION

In this paper, we proposed the unified TE framework, leveraging TE in MU-MIMO systems. Firstly, we defined the concept of TE, which encompasses definitions of multiple properties. On this basis, we put forward the TE framework,

which is capable of designing NNs with TE for MU-MIMO systems. In this framework, the various modules are plug-and-play, allowing them to be stacked to accommodate different properties and applicable for various wireless communication tasks. Taking precoding and user scheduling problems as examples, we efficiently designed corresponding AI-assisted schemes using the proposed TE framework, which demonstrates that this framework can reduce the complexity of method design. The corresponding simulation results validates the superiority of the proposed modules and the unified TE framework. In future work, we will continue to optimize the underlying code of the proposed TE modules to improve their running efficiency.

APPENDIX A PROOF OF PROPOSITION 1

We demonstrate partial conclusions in the proposition as follows

$$\sum_{k=1}^K R_k(\mathbf{H}, \mathbf{W}, \sigma^2) = \sum_{k=1}^K R_k(\pi_{K \circ 1} \mathbf{H}, \pi_{K \circ 1} \mathbf{W}, \sigma^2), \quad (41)$$

$$= \sum_{k=1}^K R_k(\pi_{N_R \circ 2} \mathbf{H}, \pi_{N_R \circ 2} \mathbf{W}, \sigma^2), \quad (42)$$

$$= \sum_{k=1}^K R_k(\pi_{N_T \circ 3} \mathbf{H}, \pi_{N_T \circ 3} \mathbf{W}, \sigma^2). \quad (43)$$

Then, the remaining conclusions in the proposition can be obtained through proof by contradiction.

We first consider the proof of (41). For convenience, we use π to denote π_K , and the sum-rate expression considering its influence is as follows

$$R_k(\pi \circ 1 \mathbf{H}, \pi \circ 1 \mathbf{W}, \sigma^2) = \log \det \left(\mathbf{I} + \mathbf{W}_{\pi(k)} \mathbf{H}_{\pi(k)}^H (\Omega'_k)^{-1} \mathbf{H}_{\pi(k)} \mathbf{W}_{\pi(k)}^H \right), \quad (44)$$

where $\Omega'_k = \sigma^2 \mathbf{I} + \sum_{i=1, i \neq \pi(k)}^K \mathbf{H}_{\pi(k)} \mathbf{W}_i^H \mathbf{W}_i \mathbf{H}_{\pi(k)}^H = \Omega_{\pi(k)}$. Thus, we have

$$\begin{aligned} R_k(\pi \circ 1 \mathbf{H}, \pi \circ 1 \mathbf{W}, \sigma^2) &= \log \det \left(\mathbf{I} + \mathbf{W}_{\pi(k)} \mathbf{H}_{\pi(k)}^H \Omega_{\pi(k)}^{-1} \mathbf{H}_{\pi(k)} \mathbf{W}_{\pi(k)}^H \right) \\ &= R_{\pi(k)}(\mathbf{H}, \mathbf{W}, \sigma^2). \end{aligned} \quad (45)$$

Substituting this expression into (41) yields its validity.

Subsequently, we consider the proof of (42) and use π to denote π_{N_R} . We define the permutation matrix $\mathbf{\Pi}$ to represent the permutation of π at the second dimension of \mathbf{H} and \mathbf{W} . In matrix $\mathbf{\Pi}$, each row contains only one element equal to 1, with all other elements being 0, and all elements 1 are located in distinct columns. Note that $\mathbf{\Pi} \mathbf{\Pi}^T = \mathbf{I}$. For $\pi \circ 2 \mathbf{H}$ and $\pi \circ 2 \mathbf{W}$, the corresponding channel and precoder of the k -th user can be expressed as $\mathbf{H}'_k = \mathbf{\Pi} \mathbf{H}_k$ and $\mathbf{W}'_k = \mathbf{\Pi} \mathbf{W}_k$. On this basis, we have

$$\begin{aligned} R_k(\pi \circ 2 \mathbf{H}, \pi \circ 2 \mathbf{W}, \sigma^2) &= \log \det \left(\mathbf{I} + \mathbf{W}'_k (\mathbf{H}'_k)^H (\Omega'_k)^{-1} \mathbf{H}'_k (\mathbf{W}'_k)^H \right) \\ &= \log \det \left(\mathbf{I} + \mathbf{\Pi} \mathbf{W}_k \mathbf{H}_k^H \mathbf{\Pi}^T (\Omega'_k)^{-1} \mathbf{\Pi} \mathbf{H}_k \mathbf{W}_k^H \mathbf{\Pi}^H \right), \end{aligned} \quad (46)$$

where $\Omega'_k = \sigma^2 \mathbf{I} + \sum_{i=1, i \neq k}^K \mathbf{\Pi} \mathbf{H}_k \mathbf{W}_i^H \mathbf{\Pi}^T \mathbf{\Pi} \mathbf{W}_i \mathbf{H}_k^H \mathbf{\Pi}^T$. According to Sylvester determinant identity that $\det(\mathbf{I} + \mathbf{A} \mathbf{B}) = \det(\mathbf{I} + \mathbf{B} \mathbf{A})$, it can be derived that

$$\begin{aligned} R_k(\pi \circ 2 \mathbf{H}, \pi \circ 2 \mathbf{W}, \sigma^2) &= \log \det \left(\mathbf{I} + \mathbf{W}_k \mathbf{H}_k^H \mathbf{\Pi}^T (\Omega'_k)^{-1} \mathbf{\Pi} \mathbf{H}_k \mathbf{W}_k^H \right). \end{aligned} \quad (47)$$

According to Woodbury matrix identity, we have $(\Omega'_k)^{-1} = \mathbf{\Pi} (\Omega_k)^{-1} \mathbf{\Pi}^T$. Substituting this expression into (47) yields $R_k(\pi \circ 2 \mathbf{H}, \pi \circ 2 \mathbf{W}, \sigma^2) = R_k(\mathbf{H}, \mathbf{W}, \sigma^2)$. Therefore, (42) holds. Similarly, it can be proved that (43) also holds.

Based on (41)-(43), Given a fixed σ , it is easy to prove that if \mathbf{W}^* is one of the optimal solutions for problem (4) based on \mathbf{H} , then $\pi_{K \circ 1} \mathbf{W}^*$, $\pi_{N_R \circ 2} \mathbf{W}^*$, and $\pi_{N_T \circ 3} \mathbf{W}^*$ are also ones of the optimal solutions for problem (4) based on $\pi_{K \circ 1} \mathbf{H}$, $\pi_{N_R \circ 2} \mathbf{H}$, and $\pi_{N_T \circ 3} \mathbf{H}$, respectively. This completes the proof.

APPENDIX B PROOF OF PROPOSITION 2

Based on **Proposition 1**, the validity of the following equation leads to the establishment of **Proposition 2**.

$$\pi_{K \circ 1} \mathbf{W} = \text{CFP}(\pi_{K \circ 1} \mathbf{H}, \pi_{K \circ 1} \mathbf{A}, \pi_{K \circ 1} \mathbf{U}, \sigma^2), \quad (48)$$

$$\pi_{N_R \circ 2} \mathbf{W} = \text{CFP}(\pi_{N_R \circ 2} \mathbf{H}, \pi_{N_R \circ [2,3]} \mathbf{A}, \pi_{N_R \circ [2,3]} \mathbf{U}, \sigma^2), \quad (49)$$

$$\pi_{N_T \circ 3} \mathbf{W} = \text{CFP}(\pi_{N_T \circ 3} \mathbf{H}, \mathbf{A}, \mathbf{U}, \sigma^2), \quad (50)$$

where $\mathbf{W} = \text{CFP}(\mathbf{H}, \mathbf{A}, \mathbf{U})$. Next, we will separately prove these equations.

We first consider the proof of (48). We use π to denote π_K and define $\mathbf{W}' = \text{CFP}(\pi_{K \circ 1} \mathbf{H}, \pi_{K \circ 1} \mathbf{A}, \pi_{K \circ 1} \mathbf{U})$. According to (6) and Woodbury matrix identity, we have $\tilde{\mathbf{W}}'_k = \mathbf{U}_{\pi(k)}^T \mathbf{A}_{\pi(k)}^* \mathbf{H}_{\pi(k)}^* (\mathbf{\Upsilon} + \mu' \mathbf{I}_N)^{-1}$, where $\mathbf{\Upsilon} = \sum_{k=1}^K \mathbf{H}_k^H \mathbf{A}_k^H \mathbf{U}_k \mathbf{A}_k \mathbf{H}_k$, $\mu' = \text{Tr}(\mathbf{U}' \mathbf{A}' \mathbf{A}'^H) = \text{Tr}(\mathbf{U} \mathbf{A} \mathbf{A}^H) = \mu$, $\mathbf{U}' = \text{blkdiag}\{\mathbf{U}_{\pi(1)}, \dots, \mathbf{U}_{\pi(K)}\}$, and $\mathbf{A}' = \text{blkdiag}\{\mathbf{A}_{\pi(1)}, \dots, \mathbf{A}_{\pi(K)}\}$. Then, we can conclude $\tilde{\mathbf{W}}'_k = \tilde{\mathbf{W}}_{\pi(k)}$, which leads to $\mathbf{W}' = \pi_{K \circ 1} \mathbf{W}$.

Subsequently, we consider the proof of (49). We use π to denote π_{N_R} . We define the permutation matrix $\mathbf{\Pi}$ to represent the permutation of π at \mathbf{H} , \mathbf{A} , and \mathbf{U} . For $\pi \circ 2 \mathbf{H}$, $\pi \circ [2,3] \mathbf{A}$, and $\pi \circ [2,3] \mathbf{U}$. The corresponding channel and auxiliary tensors of the k -th user can be expressed as $\mathbf{H}'_k = \mathbf{\Pi} \mathbf{H}_k$, $\mathbf{A}'_k = \mathbf{\Pi} \mathbf{A}_k \mathbf{\Pi}^T$, and $\mathbf{U}'_k = \mathbf{\Pi} \mathbf{U}_k \mathbf{\Pi}^T$. After permutation, the expression for the precoding matrix before scaling for the k -th user is given by $\tilde{\mathbf{W}}'_k = \mathbf{\Pi} \mathbf{U}_k^T \mathbf{A}_k^* \mathbf{H}_k^* (\mathbf{\Upsilon} + \mu' \mathbf{I}_N)^{-1}$, which leads to $\mathbf{W}' = \mathbf{\Pi} \tilde{\mathbf{W}}_k = \pi \circ 2 \mathbf{W}$. Similar to the proof of (48), (50) can be proved. This completes the proof.

APPENDIX C PROOF OF PROPOSITION 3

Similar to Appendix A, the establishment of **Proposition 3** can be proven by demonstrating the validity of the following equations

$$R_{\text{US}}(\tilde{\mathbf{H}}, \boldsymbol{\eta}, \sigma^2) = R_{\text{US}}(\pi_{\tilde{K} \circ 1} \tilde{\mathbf{H}}, \pi_{\tilde{K} \circ 1} \boldsymbol{\eta}, \sigma^2), \quad (51)$$

$$R_{\text{US}}(\tilde{\mathbf{H}}, \boldsymbol{\eta}, \sigma^2) = R_{\text{US}}(\pi_{N_R \circ 2} \tilde{\mathbf{H}}, \boldsymbol{\eta}, \sigma^2), \quad (52)$$

$$R_{\text{US}}(\tilde{\mathbf{H}}, \boldsymbol{\eta}, \sigma^2) = R_{\text{US}}(\pi_{N_T \circ 3} \tilde{\mathbf{H}}, \boldsymbol{\eta}, \sigma^2). \quad (53)$$

For (51), we have

$$R_{\text{US}}(\pi_{\circ 1} \tilde{\mathbf{H}}, \pi_{\circ 1} \boldsymbol{\eta}, \sigma^2) = \sum_{k' \in \mathcal{K}'} R_{k'}(\mathbf{H}', G_{\text{CP}}(\mathbf{H}', \sigma^2), \sigma^2), \quad (54)$$

where $\mathcal{K}' = \{\pi(k) | \eta_k = 1, k \in \tilde{\mathcal{K}}\}$ and $\mathbf{H}' = [\mathbf{H}'_{k'}]_{0, k' \in \mathcal{K}'} \in \mathbb{C}^{K \times N_{\text{R}} \times N_{\text{T}}}$. It is easy to verify that $\mathbf{H}'_{k'} = \mathbf{H}_{\pi^{-1}(k')}$. With the definition of \mathcal{K}' , we can conclude that $\mathbf{H}' = \pi_{\text{K}} \circ 1 \mathbf{H}, \pi_{\text{K}} \in \mathbb{S}_K$. Substituting this equation into (54) yields the establishment of (51). Similarly, it can be proved that (52) and (53) also holds. This completes the proof.

APPENDIX D PROOF OF PROPOSITION 4

We prove the validity of this proposition under the scenario of $D_{\text{I}} = D_{\text{O}} = 1$, and this conclusion can be easily extended to the scenario of $D_{\text{I}} > 1$ and $D_{\text{O}} > 1$. Besides, we temporarily ignore the bias \mathbf{b} and derive its pattern at the end. We reshape the weights to $\mathbf{W} \in \mathbb{R}^{M_1 \times \dots \times M_N \times M_1 \times \dots \times M_N}$ and use $\mathbf{W}_{[\mathbf{p}, \mathbf{q}]}$ to represent $\mathbf{W}_{[p_1, \dots, p_N, q_1, \dots, q_N]}$. According to [41], it can be derived that the weights satisfying multidimensional equivariance across dimensions in $\mathcal{N} = \{1, \dots, N\}$ exhibit the following pattern

$$\mathbf{W}_{[\mathbf{p}, \mathbf{q}]} = w_{\mathcal{P}} \text{ s.t. } p_i = q_i, i \in \mathcal{P}, p_{i'} \neq q_{i'}, i' \in \mathcal{N} \setminus \mathcal{P}, \quad (55)$$

where $w_{\mathcal{P}}$ is defined for each $\mathcal{P} \subseteq \mathcal{N}$ (which is equivalent to $\mathcal{P} \in \tilde{\mathcal{N}}$). The above equation implies that, for a specific set of dimensions \mathcal{P} , the elements of \mathbf{W} , which satisfy that the N -dimensional coordinate \mathbf{p} are the same as the coordinate \mathbf{q} on dimensions only in \mathcal{P} , share the same weight $w_{\mathcal{P}}$. Due to $|\mathcal{N}| = N$, there are 2^N different elements $w_{\mathcal{P}}$ in \mathbf{W} . Although this pattern is intricate, we will proceed to demonstrate its equivalence to our expression. The p_1, \dots, p_N -th element of \mathbf{Y} is given by

$$\begin{aligned} & y_{p_1, \dots, p_N} \\ &= \sum_{q_N=1}^{M_N} \sum_{q_{N-1}=1}^{M_{N-1}} \dots \sum_{q_1=1}^{M_1} \mathbf{W}_{[\mathbf{p}, (q_1, q_2, \dots, q_N)^T]} \cdot x_{q_1, \dots, q_N} \\ &= \sum_{\mathcal{P} \subseteq \mathcal{N}} w_{\mathcal{P}} \sum_{\substack{q_i = p_i, i \in \mathcal{P} \\ q_{i'} \neq p_{i'}, i' \in \mathcal{N} \setminus \mathcal{P}}} x_{q_1, \dots, q_N} \\ &= w_{\emptyset} \sum_{q_1, \dots, q_N} x_{q_1, q_2, \dots, q_N} + (w_{\{1\}} - w_{\emptyset}) \sum_{q_2, \dots, q_N} x_{p_1, q_2, \dots, q_N} + \dots \\ &\quad + (w_{\{N\}} - w_{\emptyset}) \sum_{q_1, \dots, q_{N-1}} x_{q_1, \dots, q_{N-1}, p_N} \\ &\quad + [w_{\{1,2\}} - (w_{\{1\}} - w_{\emptyset}) - (w_{\{2\}} - w_{\emptyset}) - w_{\emptyset}] \sum_{q_3, \dots, q_N} x_{p_1, p_2, q_3, \dots, q_N} \\ &\quad + \dots \\ &\quad + (w_{\{1,2, \dots, N\}} - \dots - w_{\emptyset}) x_{p_1, \dots, p_N} \\ &= \sum_{\mathcal{P} \subseteq \mathcal{N}} \hat{w}_{\mathcal{P}} \sum_{\substack{q_i = p_i, i \in \mathcal{P} \\ q_{i'}, i' \in \mathcal{N} \setminus \mathcal{P}}} x_{q_1, \dots, q_N}, \end{aligned} \quad (56)$$

where $\hat{w}_{\emptyset} = w_{\emptyset}$ and $\hat{w}_{\mathcal{P}} = w_{\mathcal{P}} - \sum_{\mathcal{U} \subset \mathcal{P}} \hat{w}_{\mathcal{U}}$. We use $\hat{\mathbf{X}}_{\mathcal{A}} \in \mathbb{R}^{M_1 \times \dots \times M_N}$, $\mathcal{A} \subseteq \mathcal{N}$ to represent the tensor obtained by applying the summation operation over the dimensions \mathcal{A} of

tensor \mathbf{X} , which is repeated over the dimensions \mathcal{A} to match the original shape. Note that $\hat{\mathbf{X}}_{\emptyset} = \mathbf{X}$. A single term in the above formula can be represented as follows

$$\hat{w}_{\mathcal{P}} \sum_{\substack{q_i = p_i, i \in \mathcal{P} \\ q_{i'}, i' \in \mathcal{N} \setminus \mathcal{P}}} x_{q_1, \dots, q_N} = \hat{w}_{\mathcal{P}} \hat{\mathbf{X}}_{\mathcal{N} \setminus \mathcal{P}[p_1, p_2, \dots, p_N]}, \quad (57)$$

Based on the above formula, we have $y_{p_1, \dots, p_N} = \sum_{\mathcal{P} \subseteq \mathcal{N}} \hat{w}_{\mathcal{P}} \hat{\mathbf{X}}_{\mathcal{N} \setminus \mathcal{P}[p_1, p_2, \dots, p_N]}$. Thus, $\text{FC}_{\text{MDE}}(\mathbf{X})$ can be expressed as

$$\begin{aligned} \text{FC}_{\text{MDE}}(\mathbf{X}) &= \sum_{\mathcal{P} \subseteq \mathcal{N}} \hat{w}_{\mathcal{P}} \hat{\mathbf{X}}_{\mathcal{N} \setminus \mathcal{P}} = \sum_{\mathcal{P} \subseteq \mathcal{N}} \hat{w}_{\mathcal{N} \setminus \mathcal{P}} \hat{\mathbf{X}}_{\mathcal{P}} \\ &= \sum_{\mathcal{P} \subseteq \mathcal{N}} (\prod_{n \in \mathcal{P}} M_n) \cdot \hat{w}_{\mathcal{N} \setminus \mathcal{P}} \hat{\mathbf{X}}_{\mathcal{P}} = \sum_{\mathcal{P} \subseteq \mathcal{N}} \bar{w}_{\mathcal{P}} \hat{\mathbf{X}}_{\mathcal{P}}, \end{aligned} \quad (58)$$

where $\bar{w}_{\mathcal{P}} = (\prod_{n \in \mathcal{P}} M_n) \cdot \hat{w}_{\mathcal{N} \setminus \mathcal{P}}$.

Subsequently, we consider the case where bias exists. We reshape the bias to $\mathbf{B} \in \mathbb{R}^{M_1 \times \dots \times M_N}$. When the elements in \mathbf{X} are all zero, (1) degenerates to

$$\mathbf{B} = \pi_{M_n} \circ_n \mathbf{B}, \forall \pi_{M_n} \in \mathbb{S}_{M_n}, \forall n \in \mathcal{N}, \quad (59)$$

which implies that $\mathbf{B} = b\mathbf{1}$. Therefore, $\text{FC}_{\text{MDE}}(\mathbf{X})$ can be formulated as $\text{FC}_{\text{MDE}}(\mathbf{X}) = \sum_{\mathcal{P} \subseteq \mathcal{N}} \bar{w}_{\mathcal{P}} \hat{\mathbf{X}}_{\mathcal{P}} + b\mathbf{1}$. This expression can be readily extended to scenarios where $D_{\text{I}} > 1$ and $D_{\text{O}} > 1$. This completes the proof.

APPENDIX E DEFINITIONS OF TENSORS AND SETS IN FC_{HOE}

The indexing of specific features of the input and output tensors can be represented as $\mathbf{X}_{[i_1, \dots, i_p, :]}$ and $\hat{\mathbf{X}}_{[o_1, \dots, o_q, :]}$, respectively. On this basis, we define $\tilde{\mathcal{N}}_{p-q}$ as the set of all non-repetitive partitions of the index set $\{o_1, \dots, o_q, i_1, \dots, i_p\}$. The number of ways to partition a set with cardinality n is $B(n)$, where $B(\cdot)$ represents the Bell number, meaning that $|\tilde{\mathcal{N}}_{p-q}| = B(p+q)$. We suppose $\mathcal{P} \in \tilde{\mathcal{N}}_{p-q}$, and the set can be expressed as

$$\mathcal{P} = \{\mathcal{O}_1, \dots, \mathcal{O}_{N_{\mathcal{O}}}, \mathcal{T}_1, \dots, \mathcal{T}_{N_{\mathcal{T}}}, \mathcal{I}_1, \dots, \mathcal{I}_{N_{\mathcal{I}}}\}, \quad (60)$$

where \mathcal{I} only contains the elements of i , \mathcal{O} only contains the elements of o , and \mathcal{T} contains both i and o . Taking $\tilde{\mathcal{N}}_{1-2}$ as an example, it contains the following sets

$$\mathcal{P}_1 = \{o_1, o_2, i_1\} \Rightarrow \mathcal{T}_1 = \{o_1, o_2, i_1\}, \quad (61)$$

$$\mathcal{P}_2 = \{\{o_1\}, \{o_2\}, \{i_1\}\} \Rightarrow \mathcal{O}_1 = \{o_1\}, \mathcal{O}_2 = \{o_2\}, \mathcal{I}_1 = \{i_1\}, \quad (62)$$

$$\mathcal{P}_3 = \{\{o_1\}, \{o_2, i_1\}\} \Rightarrow \mathcal{O}_1 = \{o_1\}, \mathcal{T}_1 = \{o_2, i_1\}, \quad (63)$$

$$\mathcal{P}_4 = \{\{o_2\}, \{o_1, i_1\}\} \Rightarrow \mathcal{O}_1 = \{o_2\}, \mathcal{T}_1 = \{o_1, i_1\}, \quad (64)$$

$$\mathcal{P}_5 = \{\{o_1, o_2\}, \{i_1\}\} \Rightarrow \mathcal{O}_1 = \{o_1, o_2\}, \mathcal{I}_1 = \{i_1\}. \quad (65)$$

Each \mathcal{P} corresponds to a tensor $\tilde{\mathbf{X}}_{\mathcal{P}}$ with a certain pattern. To better describes the pattern, we define a mapping $\psi(\cdot)$ based on each set \mathcal{P} , as follows:

$$\psi(o_s) = \begin{cases} \tilde{o}_n, & o_s \in \mathcal{O}_n \\ t_n, & o_s \in \mathcal{T}_n \end{cases}, \quad \psi(i_s) = \begin{cases} \tilde{i}_n, & i_s \in \mathcal{I}_n \\ t_n, & i_s \in \mathcal{T}_n \end{cases} \quad (66)$$

The values of matrices $\tilde{\mathbf{X}}_{\mathcal{P}}$ and \mathbf{X} are connected through the set \mathcal{P} and mapping $\psi(\cdot)$, as follows

$$\tilde{\mathbf{X}}_{\mathcal{P}[\psi(o_1), \psi(o_2), \dots, \psi(o_q), :]} \quad (67)$$

$$= \frac{1}{M^{N_I}} \sum_{\tilde{i}_1=1}^M \cdots \sum_{\tilde{i}_{N_I}=1}^M \mathbf{X}_{[\psi(i_1), \psi(i_2), \dots, \psi(i_q), :]}, \forall \tilde{o}_n, t_n \in \mathcal{M},$$

where $\mathcal{M} = \{1, \dots, M\}$. For the indexes that can not be mapped from $\psi(\cdot)$, the elements of $\tilde{\mathbf{X}}$ are set to be zeros, i.e., $\tilde{\mathbf{X}}_{\mathcal{P}[o_1, o_2, \dots, o_q]} = 0$. Taking $\tilde{\mathcal{N}}_{1-2}$ as an example, we have the following output tensors:

$$\mathcal{P}_1 : \psi(o_1) = \psi(o_2) = \psi(i_1) = t_1, \quad (68)$$

$$\mathcal{P}_2 : \psi(o_1) = \tilde{o}_1, \psi(o_2) = \tilde{o}_2, \psi(i_1) = \tilde{i}_1, \quad (69)$$

$$\mathcal{P}_3 : \psi(o_1) = \tilde{o}_1, \psi(o_2) = \psi(i_1) = t_1, \quad (70)$$

$$\mathcal{P}_4 : \psi(o_2) = \tilde{o}_1, \psi(o_1) = \psi(i_1) = t_1, \quad (71)$$

$$\mathcal{P}_5 : \psi(o_1) = \psi(o_2) = \tilde{o}_1, \psi(i_1) = \tilde{i}_1, \quad (72)$$

↓

$$\tilde{\mathbf{X}}_{\mathcal{P}_1[t_1, t_1, :]} = \mathbf{X}_{[t_1, :]}, \forall t_1 \in \mathcal{M}, \quad (73)$$

$$\tilde{\mathbf{X}}_{\mathcal{P}_2[\tilde{o}_1, \tilde{o}_2, :]} = \frac{1}{M} \sum_{\tilde{i}_1=1}^M \mathbf{X}_{[\tilde{i}_1, :]}, \forall \tilde{o}_1, \tilde{o}_2 \in \mathcal{M}, \quad (74)$$

$$\tilde{\mathbf{X}}_{\mathcal{P}_3[\tilde{o}_1, t_1, :]} = \mathbf{X}_{[t_1, :]}, \forall \tilde{o}_1, t_1 \in \mathcal{M}, \quad (75)$$

$$\tilde{\mathbf{X}}_{\mathcal{P}_4[t_1, \tilde{o}_1, :]} = \mathbf{X}_{[t_1, :]}, \forall \tilde{o}_1, t_1 \in \mathcal{M}, \quad (76)$$

$$\tilde{\mathbf{X}}_{\mathcal{P}_5[\tilde{o}_1, \tilde{o}_1, :]} = \frac{1}{M} \sum_{\tilde{i}_1=1}^M \mathbf{X}_{[\tilde{i}_1, :]}, \forall \tilde{o}_1 \in \mathcal{M}, \quad (77)$$

Based on the above expressions, we present the construction method for the five output tensors of the 1-2-order equivariant linear layer as Fig. 13, where each small box represents a feature with length D_1 , and the blank boxes represent features with all-zero elements.

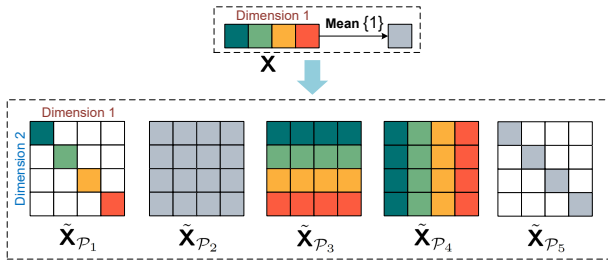


Fig. 13. The construction method for $\tilde{\mathbf{X}}_{\mathcal{P}}$ of the 1-2-order equivariant module.

Furthermore, by following the steps outlined in this appendix, we present the tensors of the 2-2 order equivariant layer in Fig. 14. In this figure, the rows and columns of the input tensor are indicated by numbers and colors, respectively. The operation $\text{Diag}\{1,2\}$ represents selecting the diagonal elements from the first and second dimensions of the tensor.

Building on the aforementioned representation of weights, we next define the representation of bias tensor $\mathbf{B}_{\mathcal{Q}}$. We define $\tilde{\mathcal{N}}_q = \{o_1, \dots, o_q\}$. Then, for $\mathcal{Q} \in \tilde{\mathcal{N}}_q$, we have

$$\mathbf{B}_{\mathcal{Q}[\psi(o_1), \psi(o_2), \dots, \psi(o_q), :]} = \mathbf{b}_{\mathcal{Q}}, \forall \tilde{o}_n \in \mathcal{M}, \quad (78)$$

where $\mathbf{b}_{\mathcal{Q}} \in \mathbb{R}^{D \times 1}$ is the learnable bias. For 1-2-order and 2-2-order equivariant layers, we have $q = 2$, which leads to

$$\mathbf{B}_{\mathcal{Q}_1[\tilde{o}_1, \tilde{o}_1, :]} = \mathbf{b}_{\mathcal{Q}_1}, \forall \tilde{o}_1 \in \mathcal{M}, \quad (79)$$

$$\mathbf{B}_{\mathcal{Q}_2[\tilde{o}_1, \tilde{o}_2, :]} = \mathbf{b}_{\mathcal{Q}_2}, \forall \tilde{o}_1, \tilde{o}_2 \in \mathcal{M}. \quad (80)$$

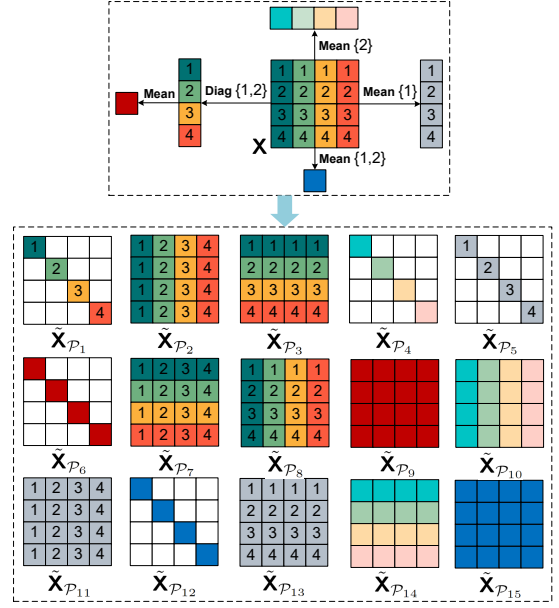


Fig. 14. The construction method for the output tensors of the 2-2-order equivariant layer.

APPENDIX F

PROOF OF PROPOSITION 6

Proposition 6 can be expressed as the following two points:

- If $g_1 : \mathbb{R}^{M \times \cdots \times M \times D_X} \rightarrow \mathbb{R}^{M \times \cdots \times M \times D_{Y'}}$ satisfies p -dimensional equivariance, $g_2 : \mathbb{R}^{M \times \cdots \times M \times D_{Y'}} \rightarrow \mathbb{R}^{M \times \cdots \times M \times D_Y}$ satisfies p - q -order equivariance, then $f = g_2 \circ g_1$ also satisfies p - q -order equivariance.
- If $h_1 : \mathbb{R}^{M_1 \times \cdots \times M_N \times D_X} \rightarrow \mathbb{R}^{M_1 \times \cdots \times M_N \times D_Y}$ satisfies N -dimensional equivariance, $h_2 : \mathbb{R}^{M_1 \times \cdots \times M_N \times D_X} \rightarrow \mathbb{R}^{D_Y}$ satisfies N -dimensional invariance, then $f = h_2 \circ h_1$ also satisfies N -dimensional invariance.

For the first point, we have

$$\begin{aligned} f(\pi_M \circ_{[1, \dots, p]} \mathbf{X}) &= g_2(g_1(\pi_M \circ_{[1, \dots, p]} \mathbf{X})) \\ &= g_2(\pi_M \circ_{[1, \dots, p]} g_1(\mathbf{X})) = \pi_M \circ_{[1, \dots, q]} g_2(g_1(\mathbf{X})) \quad (81) \\ &= \pi_M \circ_{[1, \dots, q]} f(\mathbf{X}), \forall \pi_M \in \mathbb{S}_M. \end{aligned}$$

For the second point, we have

$$\begin{aligned} f(\pi_{M_n} \circ_n \mathbf{X}) &= h_2(h_1(\pi_{M_n} \circ_n \mathbf{X})) = h_2(\pi_{M_n} \circ_n h_1(\mathbf{X})) \\ &= h_2(h_1(\mathbf{X})) = f(\mathbf{X}), \forall \pi_{M_n} \in \mathbb{S}_{M_n}, \forall n \in \mathcal{N}. \quad (82) \end{aligned}$$

This completes the proof.

APPENDIX G

CASE OF MULTIPLE OPTIMAL SOLUTIONS

In this appendix, we discuss the research paradigm proposed in Sections II-B and II-C, which involves exploiting TE of mappings from available information to optimal solution in optimization problem, under the case where the optimization problem has multiple optimal solutions.

The theory in TE framework that exploiting TE within the target mapping accommodates both single optimal solutions

and cases with multiple optimal solutions. Specifically, if the original problem has multiple optimal solutions, the optimization problem based on the permuted available information (specifically, the CSI in optimization problem of precoding) will also exhibit the same number of optimal solutions, which correspond one-to-one with the optimal solutions of the original problem through the same permutation. Thus, the mapping from available information to a certain optimal solution still satisfies TE.

Taking the problem of sum rate maximization in precoding design as an example.

$$\max_{\mathbf{W}} \sum_{k=1}^K R_k(\mathbf{H}, \mathbf{W}, \sigma^2) \quad \text{s.t.} \quad \sum_{k=1}^K \text{Tr}(\mathbf{W}_k \mathbf{W}_k^H) \leq P_T. \quad (83)$$

To simplify the description, we take the single-dimensional equivariance as an example. According to the derivation in **Appendix A**, we have the following proposition

Proposition 7. *The objective function of $\langle \mathbf{W}, \{\mathbf{H}, \sigma^2 \} \rangle_{\mathbb{P}}$ is equal to those of $\langle \pi_K \circ_1 \mathbf{W}, \{\pi_K \circ_1 \mathbf{H}, \sigma^2 \} \rangle_{\mathbb{P}}$, for all $\pi_K \in \mathbb{S}_K$. Specifically, if $\langle \mathbf{W}^*, \{\mathbf{H}, \sigma^2 \} \rangle_{\mathbb{P}}$ achieves the optimal objective function, then $\langle \pi_K \circ_1 \mathbf{W}^*, \{\pi_K \circ_1 \mathbf{H}, \sigma^2 \} \rangle_{\mathbb{P}}$ can also achieve their optimal objective functions.*

The above proposition illustrates that the optimal solutions of the optimization problem based on \mathbf{H}, σ^2 and the optimization problem based on $\pi_K \circ_1 \mathbf{H}, \sigma^2, \forall \pi_K \in \mathbb{S}_K$, have a one-to-one correspondence. Therefore, the following conclusion can be derived.

Proposition 8. *For precoding design problem (83), the number of optimal solutions for the problem based on CSI \mathbf{H}, σ^2 is the same as that for the optimization problem based on CSI $\pi_K \circ_1 \mathbf{H}, \sigma^2, \forall \pi_K \in \mathbb{S}_K$.*

If the above optimization problem has T optimal solutions, according to **Proposition 7** and **Proposition 8**, they have the following relationship: for the original problem

$$G_{\mathbb{P}(1)}(\mathbf{H}, \sigma^2) = \mathbf{W}_{(1)}^*, \quad (84)$$

$$G_{\mathbb{P}(2)}(\mathbf{H}, \sigma^2) = \mathbf{W}_{(2)}^* \quad (85)$$

...

$$G_{\mathbb{P}(T)}(\mathbf{H}, \sigma^2) = \mathbf{W}_{(T)}^*. \quad (86)$$

For the problem based on permuted CSI

$$G_{\mathbb{P}(1)}(\pi_K \circ_1 \mathbf{H}, \sigma^2) = \pi_K \circ_1 \mathbf{W}_{(1)}^*, \quad \forall \pi_K \in \mathbb{S}_K, \quad (87)$$

$$G_{\mathbb{P}(2)}(\pi_K \circ_1 \mathbf{H}, \sigma^2) = \pi_K \circ_1 \mathbf{W}_{(2)}^*, \quad \forall \pi_K \in \mathbb{S}_K, \quad (88)$$

...

$$G_{\mathbb{P}(T)}(\pi_K \circ_1 \mathbf{H}, \sigma^2) = \pi_K \circ_1 \mathbf{W}_{(T)}^*, \quad \forall \pi_K \in \mathbb{S}_K, \quad (89)$$

where $\mathbf{W}_{(1)}^*, \dots, \mathbf{W}_{(T)}^*$ are the T optimal solutions of the optimization problem based on CSI \mathbf{H}, σ^2 . $\pi_K \circ_1 \mathbf{W}_{(1)}^*, \dots, \pi_K \circ_1 \mathbf{W}_{(T)}^*$ are the T optimal solutions of the optimization problem based on CSI $\pi_K \circ_1 \mathbf{H}, \sigma^2, \forall \pi_K \in \mathbb{S}_K$. $G_{\mathbb{P}(1)}, \dots, G_{\mathbb{P}(T)}$ are the mappings from the available CSI to the T optimal solutions, respectively. This indicates that even there are multiple optimal solutions, the mapping to obtain a specific optimal solution

still satisfies the equivariance.

Furthermore, we take the optimization problem $\max_{\mathbf{x}} f(\mathbf{x})$ as an example, where

$$f(\mathbf{x}) = \max \left\{ e^{-\left(\frac{x}{a_{2,2}} - a_{1,1}\right)^2 - \left(\frac{y}{a_{1,2}} - a_{2,1}\right)^2}, e^{-\left(\frac{x}{a_{2,1}} + a_{1,2}\right)^2 - \left(\frac{y}{a_{1,1}} + a_{2,2}\right)^2} \right\}. \quad (90)$$

To simplify the description, we denote $\mathbf{A} = \begin{bmatrix} a_{1,1} & a_{1,2} \\ a_{2,1} & a_{2,2} \end{bmatrix}$.

With $\mathbf{A} = \begin{bmatrix} 1 & 2 \\ 3 & 4 \end{bmatrix}$, the objective function is shown in Fig. 15,

with two optimal solutions denoted as $\mathbf{x}_{(1)}^* = \begin{bmatrix} a_{1,1} * a_{2,2} \\ a_{2,1} * a_{1,2} \end{bmatrix} = \begin{bmatrix} 4 \\ 6 \end{bmatrix}$ and $\mathbf{x}_{(2)}^* = \begin{bmatrix} -a_{1,2} * a_{2,1} \\ -a_{2,2} * a_{1,1} \end{bmatrix} = \begin{bmatrix} -6 \\ -4 \end{bmatrix}$. As shown in Fig. 16, when we apply a permutation to the first dimension of \mathbf{A} , for instance, let $\mathbf{A}' = \pi_{\circ_1} \mathbf{A} = \begin{bmatrix} 3 & 4 \\ 1 & 2 \end{bmatrix}$, the corresponding optimal solutions become $\mathbf{x}'_{(1)} = \begin{bmatrix} 6 \\ 4 \end{bmatrix}$ and $\mathbf{x}'_{(2)} = \begin{bmatrix} -4 \\ -6 \end{bmatrix}$, where $\mathbf{x}'_{(1)} = \pi_{\circ_1} \mathbf{x}_{(1)}^*$ and $\mathbf{x}'_{(2)} = \pi_{\circ_1} \mathbf{x}_{(2)}^*$.

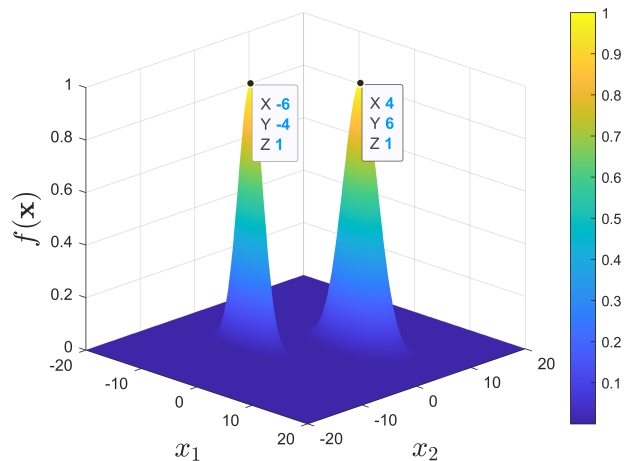


Fig. 15. Objective function with \mathbf{A} .

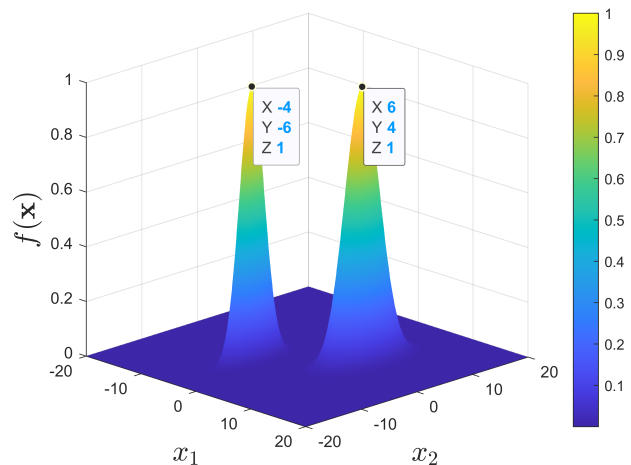


Fig. 16. Objective function with \mathbf{A}' .

Let $G_{f(1)}(\cdot)$ and $G_{f(2)}(\cdot)$ represent the mappings from \mathbf{A}

to $\mathbf{x}_{(1)}^*$ and $\mathbf{x}_{(2)}^*$, respectively, then the above process can be expressed as

$$G_{f(1)}(\mathbf{A}) = \mathbf{x}_{(1)}^*, \quad G_{f(1)}(\pi \circ_1 \mathbf{A}) = \pi \circ_1 \mathbf{x}_{(1)}^*, \quad (91)$$

$$G_{f(2)}(\mathbf{A}) = \mathbf{x}_{(2)}^*, \quad G_{f(2)}(\pi \circ_1 \mathbf{A}) = \pi \circ_1 \mathbf{x}_{(2)}^*. \quad (92)$$

The above equation verifies that the number of optimal solutions for these two optimization problems is the same, and that the mappings to their respective specific optimal solutions, such as $G_{f(1)}$ and $G_{f(2)}$, both satisfy the property of equivariance.

Another issue that needs attention is the potential impact of multiple optimal solutions on performance when using equivariant networks to fit the mapping to the optimal solution. Taking the above issue as an example, directly using \mathbf{A} as input to the equivariant NN to train for \mathbf{x}^* may cause the network to simultaneously fit both mappings $G_{f(1)}(\cdot)$ and $G_{f(2)}(\cdot)$, leading to suboptimal performance. As pointed in [26], when a specific initial value (e.g., \mathbf{x}_0) is provided as input, the network can converge to the corresponding unique optimal solution during training, thereby mitigating the performance degradation caused by multiple optimal solutions. This implies that when designing the TE network, incorporating a specific initial solution as part of the input could be a potential approach to avoid performance degradation caused by multiple optimal solutions, which can be achieved through operations such as concatenation.

APPENDIX H

LOW-COMPLEXITY PATTERN ANALYSIS

In this appendix, we provide the theoretical analysis underpinning the complexity reduction approach proposed in Section III-A, along with the final method proposed based on this analysis.

This method for reducing computational complexity and parameter count is applicable to both the multidimensional equivariant module and the high-order equivariant module. Here, we take the multidimensional equivariant module as an example, which can be rewritten as:

$$\text{FC}_{\text{MDE}}(\mathbf{X}) = \sum_{\mathcal{P} \in \bar{\mathcal{N}}} (\bar{\mathbf{X}}_{\mathcal{P}} \times \mathbf{W}_{\mathcal{P}}) + \mathbf{1} \otimes_N \mathbf{b}_{\text{MDE}}^T, \quad (93)$$

where $\bar{\mathcal{N}}$ denote the set containing all subsets of $\mathcal{N} = \{1, \dots, N\}$ (power set). The computational complexity of the module is related to the cardinality of set $\bar{\mathcal{N}}$ by the relationship $\mathcal{O}(|\bar{\mathcal{N}}|)$, where $|\bar{\mathcal{N}}| = 2^N$. As mentioned in our initial paper, extracting specific submatrices from the 2^N matrices of $\mathbf{W}_{\mathcal{P}}$ can reduce the computational complexity of this module, and it is easy to prove that this operation can still maintain the multidimensional equivariance. Considering that $\mathcal{P} \in \bar{\mathcal{N}}$ in (93), the method for *reducing complexity essentially means selecting an appropriate subset \mathcal{N}' to replace $\bar{\mathcal{N}}$* .

When $\mathcal{P} = \emptyset$, $\bar{\mathbf{X}}_{\mathcal{P}} = \mathbf{X}$ represents the tensor itself. When \mathcal{P} is a non-empty set, $\bar{\mathbf{X}}_{\mathcal{P}}$ is the mean of \mathbf{X} along the dimensions included in \mathcal{P} , characterizing the global feature of \mathbf{X} in the dimensions encompassed by \mathcal{P} . This indicates that the target of (93) is to perform linear interactions of tensor itself and the global feature from all the combinations of its dimensions.

We can categorize the global feature $\{\bar{\mathbf{X}}_{\mathcal{P}}\}_{\mathcal{P} \in \bar{\mathcal{N}}, \mathcal{P} \neq \emptyset}$ into two types: one is the global feature $\bar{\mathbf{X}}_{\mathcal{P}}$ on a single dimension ($|\mathcal{P}| = 1$), and the other is the global feature $\bar{\mathbf{X}}_{\mathcal{P}}$ across multiple dimensions ($|\mathcal{P}| > 1$). *If a module only considers features on a single dimension while ignoring features on multiple dimensions, can it be expected to achieve good performance? The answer is no for a single module, but maybe yes for a network composed of multiple stacked modules.*

We analyze using two-dimensional equivariance ($N = 2$) and $D_I = D_O = 1$ as an example, which can be generalized to any higher dimensions. For a single module, $\bar{\mathcal{N}} = \{\emptyset, \{1\}, \{2\}, \{1, 2\}\}$. Accordingly, the operation of the two-dimensional equivariant module is given by

$$\bar{\mathcal{N}} = \{\emptyset, \{1\}, \{2\}, \{1, 2\}\} :$$

$$\mathbf{Y} = w_{\emptyset} \mathbf{X} + w_1 \bar{\mathbf{X}}_{\{1\}} + w_2 \bar{\mathbf{X}}_{\{2\}} + w_{\{1,2\}} \bar{\mathbf{X}}_{\{1,2\}} + b \cdot \mathbf{1}, \quad (94)$$

$$y_{i,j} = w_{\emptyset} x_{i,j} + \frac{w_1}{M_1} \sum_{m=1}^{M_1} x_{m,j} + \frac{w_2}{M_2} \sum_{m=1}^{M_2} x_{i,m} + \frac{w_{\{1,2\}}}{M_1 M_2} \sum_{m_1=1}^{M_1} \sum_{m_2=1}^{M_2} x_{m_1, m_2} + b. \quad (95)$$

where $\mathbf{X} \in \mathbb{R}^{M_1 \times M_2}$ is the input, $\mathbf{Y} \in \mathbb{R}^{M_1 \times M_2}$ is the output, and $x_{i,j}$ and $y_{i,j}$ are the elements of \mathbf{X} and \mathbf{Y} at the i -th row and j -th column, respectively. If we retain only the global features of each individual dimension, then the set $\bar{\mathcal{N}}$ is replaced by $\bar{\mathcal{N}}_1 = \{\emptyset, 1, 2\}$.

$$\bar{\mathcal{N}}_1 = \{\emptyset, \{1\}, \{2\}\} :$$

$$\mathbf{Y} = w_{\emptyset} \mathbf{X} + w_1 \bar{\mathbf{X}}_{\{1\}} + w_2 \bar{\mathbf{X}}_{\{2\}} + b \cdot \mathbf{1}, \quad (96)$$

$$y_{i,j} = w_{\emptyset} x_{i,j} + \frac{w_1}{M_1} \sum_{m=1}^{M_1} x_{m,j} + \frac{w_2}{M_2} \sum_{m=1}^{M_2} x_{i,m} + b. \quad (97)$$

The output $y_{i,j}$ in Equation (97) contains the global features of the row and column where x is located. However, compared to the output in (95), the output in Equation (97) lacks the global feature shared across dimensions 1 and 2, which includes features from other rows and columns, i.e., $x_{m,n}, m \neq i, n \neq j$. This indicates that even if the features of other rows and columns undergo significant changes, the output $y_{i,j}$ corresponding to $x_{i,j}$ will remain unchanged, which maybe unreasonable. For example, in the case of a MU-MIMO channel, it is clearly unreasonable that arbitrary changes in the channels of other users' other antennas do not affect the transmission scheme design of certain antenna from current user. This shows that *in the case of a single layer, removing the global feature shared across multiple dimensions in the multidimensional equivariant module will cause the network to lose the ability to capture cross-dimensional global features.*

The first layer:

$$y_{i,j}^{(1)} = w_{\emptyset}^{(1)} x_{i,j} + \frac{w_1^{(1)}}{M_1} \sum_{m=1}^{M_1} x_{m,j} + \frac{w_2^{(1)}}{M_2} \sum_{m=1}^{M_2} x_{i,m} + b^{(1)}, \quad (98)$$

The second layer:

$$y_{i,j}^{(2)} = w_{\emptyset}^{(2)} y_{i,j}^{(1)} + \frac{w_1^{(2)}}{M_1} \sum_{m=1}^{M_1} y_{m,j}^{(1)} + \frac{w_2^{(2)}}{M_2} \sum_{m=1}^{M_2} y_{i,m}^{(1)} + b^{(2)}. \quad (99)$$

Then, we consider a two-layer neural network (for the sake of clarity, we ignore element-wise operations such as activation functions), as shown in equations (98) and (99). As mentioned in the previous paragraph, $y_{i,j}^{(1)}$ does not capture cross-dimensional features; it only captures the features of the row and column where $x_{i,j}$ is located. However, during the processing of the second layer, $y_{i,j}^{(2)}$ includes the features from $y_{i,j}^{(1)}$ of the corresponding row and column, where these $y_{i,j}^{(1)}$ respectively capture the features of their corresponding row and column dimensions. This enables $y_{i,j}^{(2)}$ to capture both the single dimensional features in the row and column of $x_{i,j}$ as well as the features across the two dimensions. This mechanism is similar to the receptive field mechanism of convolutional layers [50]: although a single convolutional layer has a limited receptive field, it can gradually expand its receptive field by stacking multiple convolutional layers. This illustrates that *for a network composed of multiple stacked layers, even if a single layer only possesses the ability to capture global features across individual dimensions, the network still has the potential to capture cross-dimensional global features.*

Based on the analysis above, if we need to construct a network containing L layers of equivariant modules, Where the l -th layer of the equivariant module uses the set $\bar{\mathcal{N}}_l'$ to replace $\bar{\mathcal{N}}$ in (93). We propose the following three patterns for selecting matrices (i.e., constructing subset of $\bar{\mathcal{N}}$):

- **Pattern 1:** The set $\bar{\mathcal{N}}_l'$ for each layer of the network is the same, which is

$$\bar{\mathcal{N}}_l^{\text{P1}} = \{\emptyset, \{1\}, \{2\}, \dots, \{N\}\}, \forall l. \quad (100)$$

When $N = 3$, we have $\bar{\mathcal{N}}_l^{\text{P1}} = \{\emptyset, \{1\}, \{2\}, \{3\}\}$. The computational complexity order of this module that related to N has been reduced from $\mathcal{O}(2^N)$ to $\mathcal{O}(N+1)$.

- **Pattern 2:** The set $\bar{\mathcal{N}}_l'$ for each layer of the network can be different, but must include the empty set \emptyset . The included sets must satisfy $|\mathcal{P}| \leq 1$ and need to satisfy

$$\bar{\mathcal{N}}_1^{\text{P2}} \cup \bar{\mathcal{N}}_2^{\text{P2}} \cup \dots \cup \bar{\mathcal{N}}_L^{\text{P2}} = \{\emptyset, \{1\}, \{2\}, \dots, \{N\}\}. \quad (101)$$

For example, when $N = 3$ and $L = 3$, the sets can be $\bar{\mathcal{N}}_1^{\text{P2}} = \{\emptyset, \{1\}, \{2\}\}$, $\bar{\mathcal{N}}_2^{\text{P2}} = \{\emptyset, \{2\}, \{3\}\}$, and $\bar{\mathcal{N}}_3^{\text{P2}} = \{\emptyset, \{1\}, \{3\}\}$. The above equation ensures that there is no loss of global information capture for certain dimensions or combinations of dimensions throughout the entire network. The complexity order of this module that related to N has been reduced from $\mathcal{O}(2^N)$ to $\mathcal{O}(N')$, where $N' = \frac{\sum_{l=1}^L |\bar{\mathcal{N}}_l^{\text{P2}}|}{L} \leq N + 1$.

- **Pattern 3:** The sets $\bar{\mathcal{N}}_l'$ of different layers can be different, but they only contain two elements, \emptyset and \mathcal{P}_l , where $|\mathcal{P}_l| = 1$, and they need to satisfy

$$\mathcal{P}_1 \cup \mathcal{P}_2 \cup \dots \cup \mathcal{P}_L = \{\{1\}, \{2\}, \dots, \{N\}\}. \quad (102)$$

For example, when $N = 3$ and $L = 3$, the sets can

be $\bar{\mathcal{N}}_1^{\text{P3}} = \{\emptyset, \{1\}\}$, $\bar{\mathcal{N}}_2^{\text{P3}} = \{\emptyset, \{2\}\}$, and $\bar{\mathcal{N}}_3^{\text{P3}} = \{\emptyset, \{3\}\}$. This pattern can be regarded as a special case of **Pattern 2**. The complexity order of this module that related to N has been reduced from $\mathcal{O}(2^N)$ to $\mathcal{O}(2)$.

REFERENCES

- [1] F. Rusek, D. Persson *et al.*, "Scaling up MIMO: Opportunities and challenges with very large arrays," *IEEE Signal Process. Mag.*, vol. 30, no. 1, pp. 40–60, Jan. 2013.
- [2] C.-X. Wang, X. You *et al.*, "On the road to 6G: Visions, requirements, key technologies and testbeds," *IEEE Commun. Surv. Tutor.*, vol. 25, no. 2, pp. 905–974, Secondquarter 2023.
- [3] G. Dimic and N. D. Sidiropoulos, "On downlink beamforming with greedy user selection: Performance analysis and a simple new algorithm," *IEEE Trans. Signal Process.*, vol. 53, no. 10, pp. 3857–3868, Sept. 2005.
- [4] S. S. Christensen, R. Agarwal *et al.*, "Weighted sum-rate maximization using weighted MMSE for MIMO-BC beamforming design," *IEEE Trans. Wireless Commun.*, vol. 7, no. 12, pp. 4792–4799, Dec. 2008.
- [5] Q. Shi, M. Razaviyayn *et al.*, "An iteratively weighted MMSE approach to distributed sum-utility maximization for a MIMO interfering broadcast channel," *IEEE Trans. Signal Process.*, vol. 59, no. 9, pp. 4331–4340, Sept. 2011.
- [6] X. Zhao, S. Lu *et al.*, "Rethinking WMMSE: Can its complexity scale linearly with the number of BS antennas?" *IEEE Trans. Signal Process.*, vol. 71, pp. 433–446, Feb. 2023.
- [7] B. Hochwald, C. Peel, and A. Swindlehurst, "A vector-perturbation technique for near-capacity multiantenna multiuser communication-Part II: Perturbation," *IEEE Trans. Commun.*, vol. 53, no. 3, pp. 537–544, 2005.
- [8] M. Costa, "Writing on dirty paper (corresp.)," *IEEE Trans. Inf. Theory*, vol. 29, no. 3, pp. 439–441, 1983.
- [9] L. Liu and W. Yu, "Massive connectivity with massive MIMO—Part I: Device activity detection and channel estimation," *IEEE Trans. Signal Process.*, vol. 66, no. 11, pp. 2933–2946, 2018.
- [10] K. Hornik, M. Stinchcombe, and H. White, "Multilayer feedforward networks are universal approximators," *Neural networks*, vol. 2, no. 5, pp. 359–366, 1989.
- [11] C. Yun, S. Bhojanapalli *et al.*, "Are transformers universal approximators of sequence-to-sequence functions?" *arXiv preprint arXiv:1912.10077*, 2019. [Online]. Available: <https://arxiv.org/abs/1912.10077>
- [12] K. B. Letaief, W. Chen *et al.*, "The roadmap to 6G: AI empowered wireless networks," *IEEE Commun. Mag.*, vol. 57, no. 8, pp. 84–90, Aug. 2019.
- [13] J. Kim, H. Lee *et al.*, "Deep learning methods for universal MISO beamforming," *IEEE Wireless Commun. Lett.*, vol. 9, no. 11, pp. 1894–1898, Nov. 2020.
- [14] H. Huang, Y. Peng *et al.*, "Fast beamforming design via deep learning," *IEEE Trans. Veh. Technol.*, vol. 69, no. 1, pp. 1065–1069, Jan. 2019.
- [15] S. Lu, S. Zhao, and Q. Shi, "Learning-based massive beamforming," in *IEEE Glob. Commun. Conf., (GLOBECOM)*, Dec. 2020, pp. 1–6.
- [16] W. Xia, G. Zheng *et al.*, "A deep learning framework for optimization of MISO downlink beamforming," *IEEE Trans. Commun.*, vol. 68, no. 3, pp. 1866–1880, Mar. 2020.
- [17] J. Shi, W. Wang *et al.*, "Deep learning-based robust precoding for massive MIMO," *IEEE Trans. Commun.*, vol. 69, no. 11, pp. 7429–7443, Nov. 2021.
- [18] J. Shi, A.-A. Lu *et al.*, "Robust WMMSE precoder with deep learning design for massive MIMO," *IEEE Trans. Commun.*, vol. 71, no. 7, pp. 3963–3976, Jul. 2023.
- [19] E. Björnson, M. Bengtsson, and B. Ottersten, "Optimal multiuser transmit beamforming: A difficult problem with a simple solution structure [lecture notes]," *IEEE Signal Process. Mag.*, vol. 31, no. 4, pp. 142–148, Jul. 2014.
- [20] L. Pellaco, M. Bengtsson, and J. Jaldén, "Matrix-inverse-free deep unfolding of the weighted MMSE beamforming algorithm," *IEEE Open J. Commun. Soc.*, vol. 3, pp. 65–81, Dec. 2021.
- [21] Q. Hu, Y. Cai *et al.*, "Iterative algorithm induced deep-unfolding neural networks: Precoding design for multiuser MIMO systems," *IEEE Trans. Wireless Commun.*, vol. 20, no. 2, pp. 1394–1410, Feb. 2021.
- [22] K. Wang and A. Liu, "Robust WMMSE-based precoder with practice-oriented design for massive MU-MIMO," *IEEE Wireless Commun. Lett.*, Early Access, 2024.

- [23] F. Liang, C. Shen *et al.*, "Towards optimal power control via ensembling deep neural networks," *IEEE Trans. Commun.*, vol. 68, no. 3, pp. 1760–1776, Mar. 2020.
- [24] Y. Li, S. Han, and C. Yang, "User scheduling for uplink OFDMA systems by deep learning," in *IEEE Wireless Commun. Networking Conf. (WCNC)*, Nanjing, China, Mar. 2020, pp. 1–6.
- [25] B. Xie, S. Chen *et al.*, "Learning-assisted user scheduling and beamforming for mmWave vehicular networks," *IEEE Trans. Veh. Technol.*, Early Access, 2024.
- [26] H. Sun, X. Chen *et al.*, "Learning to optimize: Training deep neural networks for interference management," *IEEE Trans. Signal Process.*, vol. 66, no. 20, pp. 5438–5453, Oct. 2018.
- [27] X. Yi, "Asymptotic spectral representation of linear convolutional layers," *IEEE Trans. Signal Process.*, vol. 70, pp. 566–581, Jan. 2022.
- [28] M. Zaheer, S. Kottur *et al.*, "Deep sets," *Neural Inf. Proces. Syst. (NeurIPS)*, Long Beach, CA, United states, Dec. 2017.
- [29] S. Ravanbakhsh, J. Schneider, and B. Póczos, "Equivariance through parameter-sharing," in *Int. Conf. Mach. Learn. (ICML)*, vol. 6, Sydney, NSW, Australia, Aug. 2017, pp. 2892–2901.
- [30] Y. Shen, J. Zhang *et al.*, "Graph neural networks for wireless communications: From theory to practice," *IEEE Trans. Wireless Commun.*, vol. 22, no. 5, pp. 3554–3569, May 2023.
- [31] X. Yi and D. Gesbert, "Topological interference management with transmitter cooperation," *IEEE Trans. Inf. Theory*, vol. 61, no. 11, pp. 6107–6130, Nov. 2015.
- [32] Y. Shen, Y. Shi *et al.*, "Graph neural networks for scalable radio resource management: Architecture design and theoretical analysis," *IEEE J. Sel. Areas Commun.*, vol. 39, no. 1, pp. 101–115, Jan. 2020.
- [33] J. Kim, H. Lee *et al.*, "A bipartite graph neural network approach for scalable beamforming optimization," *IEEE Trans. Wireless Commun.*, vol. 22, no. 1, pp. 333–347, Jan. 2023.
- [34] J. Guo and C. Yang, "Learning power allocation for multi-cell-multi-user systems with heterogeneous graph neural networks," *IEEE Trans. Wireless Commun.*, vol. 21, no. 2, pp. 884–897, Feb. 2021.
- [35] B. Zhao, J. Guo, and C. Yang, "Learning precoding policy: CNN or GNN?" in *IEEE Wireless Commun. Networking Conf. (WCNC)*, Austin, TX, USA, Apr. 2022.
- [36] S. Liu, J. Guo, and C. Yang, "Multidimensional graph neural networks for wireless communications," *IEEE Trans. Wireless Commun.*, vol. 23, no. 4, pp. 3057–3073, Apr. 2024.
- [37] S. He, J. Yuan *et al.*, "Joint user scheduling and beamforming design for multiuser MISO downlink systems," *IEEE Trans. Wireless Commun.*, vol. 22, no. 5, pp. 2975–2988, May 2023.
- [38] H. Guo, J. Li *et al.*, "A survey on space-air-ground-sea integrated network security in 6G," *IEEE Commun. Surv. Tutor.*, vol. 24, no. 1, pp. 53–87, Firstquarter 2022.
- [39] K. Pratik, B. D. Rao, and M. Welling, "RE-MIMO: Recurrent and permutation equivariant neural MIMO detection," *IEEE Trans. Signal Process.*, vol. 69, pp. 459–473, Dec. 2020.
- [40] Y. Wang, H. Hou *et al.*, "Soft demodulator for symbol-level precoding in coded multiuser MISO systems," *IEEE Trans. Wireless Commun.*, vol. 23, no. 10, pp. 14 819–14 835, Oct. 2024.
- [41] J. Hartford, D. Graham *et al.*, "Deep models of interactions across sets," in *Int. Conf. Mach. Learn. (ICML)*, vol. 5, Stockholm, Sweden, Jul. 2018, pp. 3050–3061.
- [42] N. Keriven and G. Peyré, "Universal invariant and equivariant graph neural networks," *Neural Inf. Proces. Syst. (NeurIPS)*, vol. 32, Vancouver, BC, Canada, Dec. 2019.
- [43] J. Lee, Y. Lee *et al.*, "Set transformer: A framework for attention-based permutation-invariant neural networks," in *Int. Conf. Mach. Learn. (ICML)*, vol. 97, Long Beach, CA, United states, Jun. 2019, pp. 3744–3753.
- [44] H. Maron, H. Ben-Hamu *et al.*, "Invariant and equivariant graph networks," in *Int. Conf. Learn. Represent. (ICLR)*, New Orleans, LA, United states, May. 2019.
- [45] M. Artin, *Algebra*. Pearson Education, 2011. [Online]. Available: <https://books.google.com.hk/books?id=S6GSAGAAQBAJ>
- [46] S. Ravanbakhsh, "Universal equivariant multilayer perceptrons," in *Int. Conf. Mach. Learn. (ICML)*, vol. PartF168147-11, Virtual, Online, Jul. 2020, pp. 7952–7962.
- [47] J. Kim, D. Nguyen *et al.*, "Pure transformers are powerful graph learners," *Neural Inf. Proces. Syst. (NeurIPS)*, vol. 35, pp. 14 582–14 595, New Orleans, LA, United states, Nov. 2022.
- [48] H. Maron, O. Litany *et al.*, "On learning sets of symmetric elements," in *Int. Conf. Mach. Learn. (ICML)*, vol. PartF168147-9, Virtual, Online, Jul. 2020, pp. 6690–6700.
- [49] M. Zhang, J. Gao, and C. Zhong, "A deep learning-based framework for low complexity multiuser mimo precoding design," *IEEE Trans. Wireless Commun.*, vol. 21, no. 12, pp. 11 193–11 206, 2022.
- [50] W. Luo, Y. Li *et al.*, "Understanding the effective receptive field in deep convolutional neural networks," *Advances in neural information processing systems*, vol. 29, 2016.
- [51] H. Pan and R. Kondor, "Permutation equivariant layers for higher order interactions," in *International Conference on Artificial Intelligence and Statistics (AISTATS)*, Valencia, Spain, Apr. 2023, pp. 5987–6001.
- [52] A. Vaswani, N. Shazeer, and N. Parmar, "Attention is all you need," in *Neural Inf. Proces. Syst. (NeurIPS)*, Long Beach, CA, United states, Dec. 2017.
- [53] Y. Shi, L. Lian *et al.*, "Machine learning for large-scale optimization in 6G wireless networks," *IEEE Commun. Surv. Tutor.*, vol. 25, no. 4, pp. 2088–2132, Fourthquarter 2023.
- [54] H. Mukhtar and M. El-Tarhuni, "An adaptive hierarchical QAM scheme for enhanced bandwidth and power utilization," *IEEE Trans. Commun.*, vol. 60, no. 8, pp. 2275–2284, Aug. 2012.
- [55] C. Qian, X. Fu *et al.*, "Tensor-based channel estimation for dual-polarized massive MIMO systems," *IEEE Trans. Signal Process.*, vol. 66, no. 24, pp. 6390–6403, Dec. 2018.
- [56] K. He, X. Zhang *et al.*, "Identity mappings in deep residual networks," in *Eur. Conf. Comput. Vis. (ECCV)*, vol. 9908 LNCS, Amsterdam, The Netherlands, Oct. 2016, pp. 630–645.
- [57] J. L. Ba, J. R. Kiros, and G. E. Hinton, "Layer normalization," *arXiv preprint arXiv:1607.06450*, 2016. [Online]. Available: <https://arxiv.org/abs/1607.06450>
- [58] S. Jaeckel, L. Raschkowski *et al.*, "Quadrige: A 3-D multi-cell channel model with time evolution for enabling virtual field trials," *IEEE Trans. Antennas Propag.*, vol. 62, no. 6, pp. 3242–3256, Mar. 2014.
- [59] *Technical Specification Group Radio Access Network; Study on channel model for frequencies from 0.5 to 100 GHz (Release 16)*, document 3GPP TR 38.901, Version 16.1.0, 3rd Generation Partnership Project Dec. 2019.
- [60] V. Raghavan and A. M. Sayeed, "Sublinear capacity scaling laws for sparse MIMO channels," *IEEE Trans. Inf. Theory*, vol. 57, no. 1, pp. 345–364, Jan. 2011.
- [61] D. P. Kingma and J. Ba, "Adam: A method for stochastic optimization," *arXiv preprint arXiv:1412.6980*, 2014. [Online]. Available: <https://arxiv.org/abs/1412.6980>
- [62] C. Peel, B. Hochwald, and A. Swindlehurst, "A vector-perturbation technique for near-capacity multiantenna multiuser communication-Part I: Channel inversion and regularization," *IEEE Trans. Commun.*, vol. 53, no. 1, pp. 195–202, Jan. 2005.